R. & M. No. 3320

MINISTRY OF AVIATION

AERONAUTICAL RESEARCH COUNCIL
REPORTS AND MEMORANDA

The Effect of a Cylindrical Shroud on the Performance of a Stationary Convergent Nozzle

By J. Reid

LONDON: HER MAJESTY'S STATIONERY OFFICE
1963
PRICE 16*s.* 0*d.* NET

The Effect of a Cylindrical Shroud on the Performance of a Stationary Convergent Nozzle

By J. Reid

*Reports and Memoranda No. 3320**

January, 1962

Summary.

One possible method of reducing jet noise at take-off is the use of an ejector in which the propelling nozzle discharges into a shroud and thereby induces a secondary flow. The present report describes an experiment on the aerodynamics of such systems. The primary nozzle was axisymmetric and convergent and the shrouds were cylindrical with faired convergent entries. The stagnation temperatures of the primary and secondary streams were equal and the secondary flow was entrained from the ambient static atmosphere. Ratios of jet total pressure to ambient static pressure ranged from 1·0 to 2·0.

A systematic study was made of the effect of ejector length, ejector area ratio and jet pressure ratio on the ejector performance. This was specified in terms of the ratio of secondary to primary mass flow, the velocity profile at the shroud outlet and the thrust. The variation in static pressure along the shroud wall and the distribution of total and static pressure within a shroud were also determined. No acoustic measurements were made.

The results are in fair agreement with the predictions of a simplified ejector theory which assumes uniform one-dimensional flow at the entry and outlet of the shroud and negligible skin-friction losses. The optimum shroud tested gave 15% more thrust than the unshrouded primary nozzle at a jet pressure ratio of 2·0.

1. *Introduction.*

At take-off, and during the initial phase of the subsequent climb, the noise made by large transport aircraft causes considerable hardship to quite large sections of the community. Accordingly, any device which might give a measure of relief under these conditions should be examined with care, even though it may limit the performance of the aircraft in other respects.

One such device is the ejector, of which a typical example is shown in Fig. 1†. With this arrangement the propelling nozzle exhausts into a shroud, so that the primary flow entrains from the atmosphere a secondary flow. This secondary flow is accelerated through the faired convergent entry to the shroud to a velocity (u_2) which is, in general, less than the primary jet velocity (u_1). Consequently there exists a discontinuity in the velocity profile across the shroud in the primary-nozzle exit plane. Downstream of this plane a process of turbulent mixing tends to smooth out this discontinuity so that, provided the shroud is long enough, the combined flows leave the shroud with a velocity (u_3) which is nearly uniform over the cross-section and is less than u_1. The overall

* Replaces R.A.E. Report No. Aero. 2659—A.R.C. 23,749.

† Fig. 1, in conjunction with the 'List of Symbols', also shows the system of notation used throughout the report.

effect of the shroud is, therefore, to convert a given mass flow of high-velocity air into a larger mass flow of air moving with a lower velocity. This conversion affects both the thrust and the noise level of the engine.

If we assume that the primary flow is choked, the presence of the shroud will not affect the forces on the internal surface of the primary nozzle. Neither will it affect the axial forces on the external surface of the primary nozzle, provided that the latter is suitably shaped (*see* Fig. 1). On the other hand, there will be a thrust on the shroud intake because acceleration of the secondary flow gives rise to sub-atmospheric pressures on the internal surface of this intake. The only other axial force acting on a cylindrical shroud is a drag due to skin friction on the internal surface. On balance, it seems likely that a suitably proportioned shroud will increase the thrust of the system and hence decrease the specific fuel consumption.

The effect of an ejector on noise level is less clear. At a given thrust a long shroud can reduce the effective exit velocity (relative to the unshrouded primary nozzle) by a significant factor. On the basis of the eighth-power velocity law this should lead to a marked reduction in noise level. We must remember, however, that mixing inside the shroud will produce a high turbulence level at the shroud exit and this will tend to increase the noise. Also, acoustic lagging of the shroud may be necessary to prevent radiation through the walls. If the shroud is too short to have much effect on the mean exit velocity this argument loses force. Nevertheless, in this case mixing within the shroud will be incomplete and the maximum transverse velocity gradient at the shroud exit will be reduced. This, in itself, may decrease the noise level.

To sum up, there are good reasons to believe that an ejector can increase the thrust, decrease the specific fuel consumption and attenuate the noise of a given engine. These are very desirable advantages, but against them we must weigh certain disadvantages.

The most serious of these are the length, diameter and weight of the shroud. Assuming that the shroud length is about ten times the primary nozzle diameter it is clear that a nacelle type of installation is precluded. If, however, we consider a large aircraft of slender delta planform with the engines installed well inboard it may be possible to bury the greater part of the engine and ejector in the wing, particularly if the latter has a blunt trailing edge. The excess weight is still a problem since, although the gas pressures and temperatures are relatively low, the shroud is subjected to high noise levels with the attendant risk of fatigue failure. Special methods of construction may, therefore, be required but, even so, the weight per unit length should compare favourably with that of a normal engine jet pipe.

The situation is much more favourable to the ejector if, instead of an axisymmetric configuration, we suppose the primary nozzle and shroud to be rectangular in cross-section, the width of the rectangle being large relative to the height. The dimension analogous to 'primary-nozzle diameter' is then 'primary-nozzle height' so that, for a given thrust and comparable mixing, the shroud is shorter and lighter and the installation problem less severe.

A further problem arises in that noise suppression is only needed at low flight speeds. Moreover, the convergent primary nozzle and subsonic shroud intake shown in Fig. 1 would give rise to a prohibitive loss in thrust at high subsonic or supersonic cruising speeds. The solution to this problem lies in a mechanically variable system which converts the primary nozzle into a convergent-divergent nozzle and simultaneously shuts the secondary intake shortly after take-off. The practical details may prove troublesome but it is not difficult to envisage a design which meets these requirements, at least in principle, for a 'two-dimensional' ejector.

2. *The Plan of the Experiment.*

It is evident that an assessment of the ejector as a practical noise suppressor must be based on both acoustic and aerodynamic data. As the total volume of experimental work is quite large, and as the techniques and apparatus required in these two fields are quite distinct, it was decided at the outset to divide the programme into two parts. The acoustic measurements (including turbulence data) are being made by a team working at Southampton University. The aerodynamic measurements have been made at the Royal Aircraft Establishment and these form the subject of the present paper.

The basic configuration tested (Fig. 1) is an axisymmetric convergent nozzle exhausting into a cylindrical shroud which has a bellmouth entry. The secondary flow induced through this entry comes from the ambient static atmosphere. This design was chosen because it is the simplest geometrical configuration which satisfies the basic requirements of an aircraft ejector at take-off. It is, however, not necessarily the optimum design.

In drawing up the test programme, three quantities were selected to specify the aerodynamic performance of an ejector. These are (*see* 'List of Symbols'); the mass-flow parameter (λ), the thrust parameter (σ) and the velocity distribution at the shroud outlet. Referring to Fig. 1 it will be apparent that each of these depends on five independent variables; namely, the approach length ratio (l/d_1), mixing-length ratio (L/d_1), ejector area ratio (a_2/a_1), jet pressure ratio ($_tp_1/p_\infty$) and jet temperature ratio ($_tT_2/_tT_1$). The prime object of the experiment was to study systematically the relationships between these two sets of quantities (with $_tT_2/_tT_1 = 1$).

These data, supplemented by the acoustic measurements, provide a factual basis for the assessment of an ejector as a thrust augmenter and noise suppressor. They should also help in correlating the noise generated by a jet with the velocity profile at the nozzle outlet. They do not, however, throw much direct light on the details of the turbulent mixing process within the shroud. This process is of considerable interest as, quite apart from its bearing on noise, it affords a relatively simple model of a general type of flow which occurs frequently in aerodynamics. The opportunity was therefore taken to investigate it further by means of radial pitot and static traverses at several axial stations between the primary nozzle and the shroud outlet. These profiles, which were measured on one shroud only, and at one value of jet pressure ratio, were supplemented by measurement of the static-pressure distribution along the walls of two shrouds over a range of jet pressure ratio.

The experimental results were compared, where possible, with the simple one-dimensional ejector theory outlined in the next section.

3. *A Simple Ejector Theory.*

On the basis of certain simplifying assumptions the problem of the flow through a cylindrical ejector can be solved by a straightforward application of the equations of continuity, momentum and energy. Details of the analysis are given in Appendix I. The present discussion is confined to a few points of general interest.

Consider first the implications of the six assumptions on which the theory is based. These are (*see* Fig. 1):

(1) $d_0 = d_1$.

(2) $_tp_2 = p_\infty$.

(3) Uniform flow at planes [1] and [2].

(4) $_tT_1 = _tT_2$.

(5) Uniform flow at plane [3].

(6) No skin friction.

The first three assumptions correspond reasonably well to conditions in a practical ejector. The fourth is introduced because it simplifies the algebra and also corresponds to the conditions of the experiment. The equations are, however, still soluble when ${}_tT_1$ is not equal to ${}_tT_2$. The assumptions which limit the value of the analysis are (5) and (6) because they are, to some extent, incompatible. If the shroud is long enough the flow will be nearly one-dimensional at the exit, but the skin friction will not be negligible. Conversely, if the shroud is short enough we may neglect skin friction, but the flow will not be one-dimensional at the exit. The only way to resolve this paradox is to analyse in detail the mixing process within the shroud. The present theory does not do this. Accordingly it is to be regarded only as a first approximation to the truth. One result of the restrictive assumptions is that the analysis yields no information on the effect of L/d_1. This is a serious shortcoming but, even so, the theoretical predictions with regard to the effect of ${}_tp_1/p_\infty$ and a_2/a_1 are of considerable value.

Appendix I also clarifies the boundary conditions of the problem. Briefly, the position is this. For sufficiently small values of ${}_tp_1/p_\infty$ (which must, of course, be greater than unity) the flow is subsonic throughout and the boundary conditions are:

Phase I

$$M_1 < 1.\ M_2 < 1.\ M_3 < 1.\ \frac{p_2}{p_1} = 1.\ \frac{p_3}{p_\infty} = 1.$$

As ${}_tp_1/p_\infty$ is continuously increased the primary nozzle eventually chokes while the secondary inlet and shroud exit remain unchoked. This is Phase II, for which the boundary conditions are:

Phase II

$$M_1 = 1.\ M_2 < 1.\ M_3 < 1.\ \frac{p_2}{p_1} \leqslant 1.\ \frac{p_3}{p_\infty} = 1.$$

Further increase in ${}_tp_1/p_\infty$ results eventually in the secondary inlet and shroud outlet choking simultaneously. This marks the start of Phase III for which the boundary conditions are:

Phase III

$$M_1 = 1.\ M_2 = 1.\ M_3 = 1.\ \frac{p_2}{p_1} < 1.\ \frac{p_3}{p_\infty} \geqslant 1.$$

Thus, as the jet pressure ratio is increased steadily and without limit, the flow passes through three physically distinct phases, each of which has its own characteristic set of boundary conditions.

The results of the calculations in Appendix I are shown in Figs. 2 and 3. In Fig. 2 the mass-flow parameter (λ) is plotted as a function of ${}_tp_1/p_\infty$ and a_2/a_1, while Fig. 3 gives the corresponding curves for the thrust parameter (σ). λ is defined as $(Q_2/Q_1)(a_1/a_2)\sqrt{({}_tT_2/{}_tT_1)}$ largely for reasons of convenience. With this definition the variation in λ with a_2/a_1 is a good deal less than it would be if the simpler and more natural ratio Q_2/Q_1 were used. We note also (Fig. 3) that, theoretically, a shroud of suitable proportions leads to a marked increase in thrust relative to the unshrouded primary nozzle.

4. *The Experimental Rigs and Models.*

4.1. *The Experimental Rigs.*

The simple rig shown in Fig. 4 was used for the whole experiment, with the exception of the thrust measurements. With this arrangement atmospheric air was compressed to a maximum stagnation

pressure of 2 atm. abs., cooled to about 20°C in a water cooler and finally delivered to the primary nozzle which was bolted to the end of a straight length of the 6 in. diameter supply pipe. The supply pressure was controlled by a valve and bleed and measured by a single axial stagnation point slightly upstream of the nozzle. The stagnation temperature, which could be controlled roughly by varying the water flow through the cooler, was measured by a copper-constantan thermo-couple. The primary air supply was undried.

To support the ejector shroud two parallel bars were bolted to the flange of the primary nozzle. Two frames were clamped to these bars. Each of these frames carried three radial adjusting screws which operated pads bearing on the outside of the shroud. By turning these screws the shroud axis could be brought into coincidence with the axis of the primary nozzle. This adjustment was made carefully with the aid of suitable gauges. The shroud was located in the correct axial position by sliding the frames along the bars and then clamping them with the screws shown.

It was not possible to measure forces with this rig. Accordingly, the thrust data were obtained by transferring the models to No. 16 (Jet Interference) Tunnel which is equipped with a suitable balance. This involved the use of a smaller supply pipe for the primary air (3 in. diameter) and a slightly modified approach section to the primary nozzle, but otherwise the models used on the two rigs were identical. As the Jet Interference Tunnel has been described fully elsewhere[1] only the relevant features will be mentioned here.

Briefly, the primary nozzle and shroud are attached to one end of a long cylindrical tube called the centrebody. The other end of this centrebody is connected to a large co-axial slotted drum which is surrounded by a plenum chamber. The primary air is supplied to this plenum chamber and passes radially through the slots, into the drum, and thence through the centrebody to the primary nozzle. The complete central assembly comprising drum, centrebody, primary nozzle and shroud is supported by three sets of ball bearings and is free to slide axially between limit stops. The thrust is measured by a simple device consisting of a piston and cylinder, in which the axial force is balanced automatically by hydraulic pressure. This unit was calibrated directly by weights and, as a further check, the measured thrust of a convergent nozzle was compared with the exit momentum determined by velocity traverses. The two values agreed within one per cent.

It should, perhaps, be emphasised that although the Jet Interference Tunnel is normally used as a supersonic tunnel, in the present application there was no external flow. The working section was left open and the secondary flow induced from the static atmosphere.

4.2. *The Models.*

One primary nozzle was used throughout the experiment. It was of the convergent, axisymmetric type and consisted of two parts; an approach section and a throat section (Fig. 4). The approach section was made out of mild steel, shaped internally in the form of a quadrant (in the meridian plane). The throat section consisted simply of a short cylindrical length of thin brass tube. Its purpose was twofold. Firstly it formed one wall of the annular entry duct for the secondary flow, and secondly it prevented the sub-atmospheric pressures in that duct from giving rise to a drag force on the primary nozzle. Two static-pressure points were installed in the wall of the throat section close to the exit plane. One measured the static pressure in the throat of the primary nozzle (p_1) and the other the static pressure in the secondary entry duct (p_2). The pressure leads to these points were completely buried in the wall so that they did not interfere with either the primary or secondary flow.

The ejector shrouds were made of 14 S.W.G. mild-steel sheet rolled and welded to form a cylindrical tube. Each tube was provided with a bellmouth entry, also made of mild steel. In the meridian plane these entries were shaped internally in the form of a quadrant with a radius of 1 in. (Fig. 4). Seventeen shrouds were tested in all, the geometrical details being shown in Table 1.

TABLE 1

Group	l/d_1	L/d_1	a_2/a_1
1	0·1	6	1·10
	0·3	6	1·10
	0·5	6	1·10
2	0·5	3	1·10
	0·5	6	1·10
	0·5	12	1·10
	0·5	20	1·10
	0·5	32	1·10
3	0·5	3	1·93
	0·5	6	1·93
	0·5	12	1·93
	0·5	20	1·93
	0·5	32	1·93
4	0·5	3	2·90
	0·5	6	2·90
	0·5	12	2·90
	0·5	20	2·90
	0·5	32	2·90

N.B. The shroud with $l/d_1 = 0{\cdot}5$, $L/d_1 = 6$ and $a_2/a_1 = 1{\cdot}10$ occurs twice in this table.

It will be noted that in Table 1 the shrouds are divided into four groups, in each of which one only of the three geometrical parameters is varied. These four groups serve to determine the separate effects of l/d_1, L/d_1 and a_2/a_1 on the performance of the ejector.

5. *Details of the Experiment.*

5.1. *Experimental Conditions.*

It is convenient to summarise here the basic conditions of the experiment. Briefly, one convergent axisymmetric primary nozzle was used in conjunction with seventeen cylindrical shrouds (Fig. 4 and Table 1). The jet pressure ratio ($_tp_1/p_\infty$) ranged from 1·0 to a maximum value of 2·0 but the jet temperature ratio ($_tT_2/_tT_1$) was approximately equal to unity throughout the tests. Both the primary and secondary air supplies were undried, the latter being entrained from the ambient static atmosphere. Within this framework the experimental measurements fall under five separate heads, each of which is discussed below.

5.2. *Primary and Secondary Mass Flows.*

We consider first the measurement of the primary mass flow. In Appendix II {equation (32)} it is shown that,

$$\frac{Q_1\sqrt{_tT_1}}{a_1{}_tp_1}\sqrt{\frac{R}{\gamma}} = C_{D1}\frac{p_1}{_tp_1}M_1\sqrt{\left(1+\frac{\gamma-1}{2}M_1^2\right)} \qquad (1)$$

where C_{D1} (the primary discharge coefficient) is constant with respect to the mass flow through the nozzle provided that the density and velocity profiles are also constant. Moreover (Appendix II and Fig. 4) p_1 and ${}_tp_1$ are measured quantities and M_1 is related to $p_1/{}_tp_1$ by the usual equation for isentropic flow. Hence $(Q_1\sqrt{{}_tT_1}/a_1{}_tp_1)\sqrt{(R/\gamma)}$ is determined once C_{D1} is known.

To find C_{D1} the primary nozzle was run at a jet pressure ratio $({}_tp_1/p_\infty)$ of 1·85 with the ejector shroud removed. Pitot and static traverses were made across four perpendicular radii in the nozzle exit plane and the mean variation in $p/{}_tp_1$ and M with r/r_1 hence determined. The non-dimensional primary mass flow was then calculated by numerical integration using equation (31) of Appendix II, i.e.,

$$\frac{Q_1\sqrt{{}_tT_1}}{a_1{}_tp_1}\sqrt{\frac{R}{\gamma}} = 2\int_0^1 \frac{p}{{}_tp_1} M \sqrt{\left(1+\frac{\gamma-1}{2}M^2\right)}\,\zeta\,d\zeta \tag{2}$$

where

$$\zeta = \frac{r}{r_1}.$$

Substitution of the measured values in equation (1) above gave $C_{D1} = 0{\cdot}982$. Previous experience with similar convergent nozzles has shown that the discharge coefficient does not vary appreciably over a range of Mach number from 0·4 to 1·0. Throughout the subsequent experiments with shrouds the primary mass flow was therefore calculated using equation (1) with $C_{D1} = 0{\cdot}982$.

A similar method was used to determine the secondary mass flow. The relevant formulae are,

$$\frac{Q_2\sqrt{{}_tT_2}}{a_2{}_tp_2}\sqrt{\frac{R}{\gamma}} = C_{D2}\frac{p_2}{{}_tp_2} M_2 \sqrt{\left(1+\frac{\gamma-1}{2}M_2^2\right)} \tag{3}$$

and

$$\frac{Q_2\sqrt{{}_tT_2}}{a_2{}_tp_2}\sqrt{\frac{R}{\gamma}} = 2\int_0^1 \frac{p}{{}_tp_2} M \sqrt{\left(1+\frac{\gamma-1}{2}M^2\right)}\,\xi\,d\xi \tag{4}$$

where

$$\xi = \sqrt{\frac{r^2-r_0^2}{r_3^2-r_0^2}}.$$

In this case, however, C_{D2} was determined separately for each of the three values of a_2/a_1 at two jet pressure ratios. One shroud $(L/d_1 = 12)$ was selected from each of Groups 2, 3 and 4 (Table 1) and the secondary annulus traversed with both a pitot and a static tube at jet pressure ratios of 1·5 and 2·0. The traverses were made across one radius only, 0·4 in. upstream of the primary-nozzle exit plane. The measured values of C_{D2} are shown in Table 2.

TABLE 2

$\frac{a_2}{a_1}$	$\frac{{}_tp_1}{p_\infty}$	C_{D2}	$(C_{D2})_{\text{mean}}$
1·10	1·5 2·0	0·971 0·973	0·972
1·93	1·5 2·0	0·958 0·962	0·960
2·90	1·5 2·0	0·950 0·950	0·950

In the test programme the secondary mass flow was calculated by substituting the appropriate mean values of C_{D2} in equation (3).

The primary and secondary mass flows were measured for each of the seventeen shrouds at jet pressure ratios ranging from 1·0 to 2·0. The mass-flow parameter $\lambda = (Q_2/Q_1)(a_1/a_2)\sqrt{({}_tT_2/{}_tT_1)}$ follows immediately from these measurements.

5.3. *Velocity Profiles at the Shroud Outlet.*

Separate pitot and static traverses were made across four perpendicular radii in the exit plane of each shroud. For this purpose a pitot tube 0·5 mm in diameter and a static tube 1 mm in diameter were used. Both were operated by an accurate micrometer traverse gear. The mean velocity corresponding to each value of r/r_3 was taken as the arithmetic average of the velocities measured on the four radii. All the values of u/u_c and u/u^* quoted in the text and figures are mean values unless the contrary is explicitly stated. The outlet profiles were measured at the following values of jet pressure ratio (*see* Table 1).

Group 1

$${}_tp_1/p_\infty = 1{\cdot}65.$$

Group 2

$${}_tp_1/p_\infty = 1{\cdot}35,\ 1{\cdot}65 \text{ and } 2{\cdot}00.$$

Groups 3 and 4

$${}_tp_1/p_\infty = 2{\cdot}00.$$

5.4. *Thrust.*

With the fifteen shrouds comprising Groups 2, 3 and 4, the thrust of the system {Appendix II, equation (34)} was measured directly by a balance at jet pressure ratios of 1·4, 1·6, 1·8 and 2·0. For reference purposes the thrust of the unshrouded primary nozzle was also measured at the same values of jet pressure ratio.

5.5. *Distribution of Static Pressure along the Shroud Wall.*

A row of static-pressure points was installed along one generator of two of the shrouds (Group 2, $L/d_1 = 12$ and 32). By this means the variation in pressure along the shroud wall was measured with ${}_tp_1/p_\infty$ equal to 1·2, 1·4, 1·6, 1·8 and 2·0.

5.6. *Profiles within the Shroud.*

One shroud (Group 2, $L/d_1 = 12$) was selected to study in more detail the development of mixing between the primary and secondary streams. Pitot and static traverses were made across one radius at seven equally spaced axial stations including the primary-nozzle outlet and the shroud outlet. For these tests the jet pressure ratio was equal to 1·65. The apparatus used was similar to that described in Section 5.3.

6. *Discussion of Results.*

6.1. *The Effect of Undried Air.*

As mentioned previously (Section 5.1) both the primary and secondary air supplies were undried. Consequently, when the atmosphere was humid and the jet pressure ratio large, the static temperature within the shroud fell slightly below the dew-point temperature and condensation occurred. On occasions a thin 'fog' was visible in the jet issuing from the shroud outlet and it was noted that condensation was apparently confined to the primary stream.

No attempt was made to investigate in detail the effects of condensation on the performance of the ejector. However, in the course of the experiment a few runs were repeated several times and no difference could be detected between the results obtained when 'fog' was visible in the exhaust and the results obtained when it was not. This is to be expected since the flow within the shroud is largely subsonic so that the possibility of condensation shocks does not arise.

6.2. *Asymmetry.*

As a rule the distribution of velocity in the exit plane of each shroud was not axisymmetric. Examples of the asymmetry pattern are shown in Fig. 5 for three of the shrouds of Group 2 ($L/d_1 = 6$, 12 and 20). In this figure the top graph ($L/d_1 = 6$) is typical of the most asymmetric profile encountered, while the bottom figure illustrates the most symmetric profile. A marked improvement in symmetry with increase in L/d_1 is to be observed in Fig. 5 and this trend was noted with all the shrouds. On the other hand changes in either a_2/a_1, l/d_1 or ${}_tp_1/p_\infty$ had very little effect.

The asymmetry pattern (i.e., the relative position of the four curves in Fig. 5) varied slightly from shroud to shroud in an apparently random fashion. In general, however, at a given value of r/r_3 the velocity tended to be greatest on the top radius and least on the bottom radius. The asymmetry pattern measured with a given shroud operating at a given jet pressure ratio could be reproduced with fair accuracy even after the lapse of some months.

Attempts were made to trace the cause of the lack of symmetry observed with the shorter shrouds. In one experiment the axis of the shroud was deliberately inclined at an angle of one degree to the axis of the primary nozzle, but this had no significant effect. In another experiment the shroud axis was moved laterally through 0·05 in. but maintained parallel to the axis of the primary nozzle. Once again no change in asymmetry could be detected. Further, the velocity distribution at the outlet of the primary nozzle was checked and found to be axisymmetric within the limits of measurement.

In view of these findings it was concluded that the turbulent mixing process within the shroud is inherently unstable in the sense that it magnifies minute departures from perfect axial symmetry existing at the primary-nozzle outlet and shroud inlet. This tendency to instability is probably accentuated by the positive pressure gradient along the shroud.

In the present experiment the effects of asymmetry at the shroud outlet were largely offset by traversing across four perpendicular radii and calculating the average velocity at a given radial distance from the axis. As explained in Section 5.3 the results are presented in terms of these mean values.

6.3. *The Effect of l/d_1 on the Mass-Flow Parameter (λ) and the Velocity Distribution at the Shroud Outlet.*

The parameter l/d_1 largely determines the initial velocity profile of the entrained secondary flow but, apart from this, it has no direct action on the actual mixing process within the shroud. We would, therefore, expect the performance of the ejector to be relatively insensitive to the magnitude of l/d_1, and this conclusion was confirmed experimentally using the three shrouds comprising Group 1 (Table 1). The evidence is presented in Figs. 6 and 7.

Fig. 6 shows the variation in λ with ${}_tp_1/p_\infty$ when l/d_1 is equal to 0·1, 0·3 and 0·5. It will be seen that the curves for $l/d_1 = 0{\cdot}3$ and 0·5 are practically coincident. Rather surprisingly, the corresponding curve for $l/d_1 = 0{\cdot}1$ lies a little below these. However, this curve is probably slightly in error because the secondary discharge coefficient ($C_{D\,2}$) was measured with $l/d_1 = 0{\cdot}5$ only (*see*

Section 5.2) and in calculating λ it was assumed that $C_{D\,2}$ does not vary with l/d_1. This assumption is probably not strictly valid when the approach length is very short ($l/d_1 = 0{\cdot}1$).

Fig. 7 shows the velocity distribution at the outlet of the shroud with l/d_1 equal to $0{\cdot}1$, $0{\cdot}3$ and $0{\cdot}5$, and ${}_tp_1/p_\infty$ equal to $1{\cdot}65$. It is evident that, within this range, l/d_1 has very little effect on the outlet profile.

It follows from the results presented in Figs. 6 and 7 that the thrust also is practically independent of l/d_1 and it was considered unnecessary to check this point experimentally. Effectively, therefore, the performance of the ejector is determined by three variables; L/d_1, a_2/a_1 and ${}_tp_1/p_\infty$.

The remainder of the experiment was concerned mainly with the effect of these three variables on the mass-flow parameter, the thrust parameter and the shroud-outlet profiles. For this investigation the fifteen shrouds comprising Groups 2, 3 and 4 of Table 1 were used and it will be noted that each of these shrouds has l/d_1 equal to $0{\cdot}5$. This value was chosen to ensure uniform one-dimensional flow in the secondary inlet annulus and hence accurate measurement of the secondary mass flow (Q_2).

6.4. *The Effect of ${}_tp_1/p_\infty$, L/d_1 and a_2/a_1 on the Mass-Flow Parameter* (λ).

It is shown in Appendix II (equation 33) that, provided the primary and secondary streams are uniform prior to mixing,

$$\lambda = \frac{p_2}{p_1}\frac{M_2}{M_1}\frac{\sqrt{\left(1+\frac{\gamma-1}{2}M_2^2\right)}}{\sqrt{\left(1+\frac{\gamma-1}{2}M_1^2\right)}}. \tag{5}$$

This equation, together with the usual relations for isentropic flow and the boundary conditions, enables the quantities M_1, M_2 and p_2/p_1 to be readily calculated for given values of λ and ${}_tp_1/p_\infty$. Thus the mass-flow parameter affords a very convenient means of expressing in concise form the initial state of the primary and secondary streams before mixing starts. In particular it should be noted that when ${}_tp_1/p_\infty$ is nearly equal to unity so that M_1 and M_2 are small and $p_2/p_1 = 1$, equation (5) above reduces to the approximate relation,

$$\lambda = \frac{M_2}{M_1}. \tag{6}$$

In this section we shall be concerned mainly with the effect of ${}_tp_1/p_\infty$, L/d_1 and a_2/a_1 on λ. However, since λ is not measured directly, it may prove helpful by way of introduction to consider first the effect of ${}_tp_1/p_\infty$ on M_1 and M_2.

A typical example of the variation in M_1 and M_2 with ${}_tp_1/p_\infty$ is shown in Fig. 8a for one of the shrouds of Group 2 ($L/d_1 = 12$). We note that M_2 increases steadily with ${}_tp_1/p_\infty$ and is subsonic over the whole of the range. M_1 on the other hand reaches unity when ${}_tp_1/p_\infty = 1{\cdot}65$ and thereafter remains constant. The ratio p_2/p_1 (which is not plotted) is equal to unity provided that ${}_tp_1/p_\infty$ is less than $1{\cdot}65$ but decreases at higher values of the jet pressure ratio. Comparing this behaviour with the simple ejector theory outlined in Section 3 it is clear that the point where ${}_tp_1/p_\infty = 1{\cdot}65$ marks transition from Phase I to Phase II. Throughout the tests the jet pressure ratio corresponding to this transition point lay between $1{\cdot}65$ and $1{\cdot}85$ depending on the shroud geometry. The available jet pressure ratio being insufficient for operation in Phase III we are, therefore concerned only with operation in Phases I and II.

Fig. 8a is typical of the results obtained with all the shrouds tested with two exceptions; namely, the shortest shrouds of Groups 3 and 4 ($L/d_1 = 3$). The relevant curves for these two shrouds are shown in Figs. 8b and 8c respectively. It will be noted that the variation in M_1 shown in these two figures is normal but the variation in M_2 is irregular. In both cases there is a fairly abrupt increase in M_2 near the point where the primary jet chokes. In addition, both these shrouds gave rise to a very intense discrete-frequency noise which almost masked the usual jet roar. This observation may have some bearing on the anomalous aerodynamic behaviour but, on the other hand, the shortest shroud of Group 2 also generated intense discrete-frequency noise and the M_2 curve for this shroud was quite normal. The phenomenon was presumably caused by instability of the flow within the shroud which gave rise to 'organ pipe' resonance. It was not investigated in detail because the shrouds concerned were too short to be of much practical interest. However, the noise aspect is discussed further in Section 7.

The effect of L/d_1 and ${}_tp_1/p_\infty$ on λ is shown in Fig. 9 for the shrouds of Group 2 ($a_2/a_1 = 1{\cdot}10$). The corresponding curves for the shrouds of Group 3 ($a_2/a_1 = 1{\cdot}93$) and Group 4 ($a_2/a_1 = 2{\cdot}90$) are presented in Figs. 10 and 11 respectively. Also shown on these three graphs are the theoretical values of λ calculated by means of the simple ejector theory presented in Appendix I. For the reasons previously given (Section 3) these theoretical values depend on ${}_tp_1/p_\infty$ and a_2/a_1 but not on L/d_1.

Referring first to Fig. 9 we see that as L/d_1 is increased with ${}_tp_1/p_\infty$ constant, λ increases rapidly at first, then reaches a peak, and finally decreases slowly. Moreover, even at the peak of each curve, the experimental values of λ lie below the corresponding theoretical values. This discrepancy is due to the two main assumptions of the theory (a uniform velocity profile at the shroud outlet and zero skin friction) since, in practice, these assumptions cannot be satisfied simultaneously. Presumably the slow decrease in λ to the right of the peak is caused by the effects of skin friction. Conversely, the rapid decrease in λ to the left of the peak is caused by incomplete mixing. In Fig. 9 we note also that, at a given value of L/d_1, an increase in ${}_tp_1/p_\infty$ results in an appreciable decrease in λ with the shorter shrouds but this effect becomes less noticeable as the shroud length increases.

The results for the shrouds of Group 3 ($a_2/a_1 = 1{\cdot}93$) and Group 4 ($a_2/a_1 = 2{\cdot}90$) shown in Figs. 10 and 11 respectively are very similar to those discussed above. To facilitate comparison the data on λ_{max} are tabulated below.

TABLE 3

$\frac{a_2}{a_1}$	$\frac{{}_tp_1}{p_\infty}$	λ_{max}	λ_{theo}	$\frac{\lambda_{max}}{\lambda_{theo}}$	$\left(\frac{L}{d_1}\right)_{\lambda=\lambda_{max}}$
1·10	1·2	0·393	0·420	0·94	9
	2·0	0·371	0·433	0·86	15
1·93	1·2	0·372	0·403	0·92	12
	2·0	0·347	0·397	0·87	18
2·90	1·2	0·355	0·383	0·93	15
	2·0	0·330	0·369	0·89	21

To summarise, we conclude from Figs. 9, 10 and 11 that λ depends primarily on L/d_1, the effects of ${}_tp_1/p_\infty$ and a_2/a_1 being of secondary importance. We conclude also, from Table 3, that for each combination of ${}_tp_1/p_\infty$ and a_2/a_1 the maximum value of λ is 86 to 94 per cent of the theoretical figure. The corresponding values of L/d_1 vary with both ${}_tp_1/p_\infty$ and a_2/a_1 but always lie between 9 and 21.

6.5. *The Effect of ${}_tp_1/p_\infty$, L/d_1 and a_2/a_1 on the Velocity Distribution at the Shroud Outlet.*

To investigate the effect of ${}_tp_1/p_\infty$ on the outlet velocity profiles the five shrouds of Group 2 ($a_2/a_1 = 1{\cdot}10$) were employed. The profile at the outlet of each of these shrouds was measured with ${}_tp_1/p_\infty$ equal to 1·35, 1·65 and 2·00. The results are shown in Fig. 12a to e in which the profiles are plotted with reference to the centreline velocity (u_c). We note firstly that, in each case, ${}_tp_1/p_\infty$ has relatively little effect on the velocity distribution. Moreover, even the small effect evident with the shorter shrouds tends to decrease with increase in shroud length (compare Fig. 12c, d and e). As a rule, at a given value of r/r_3, u/u_c decreases as ${}_tp_1/p_\infty$ increases but this rule is not universally valid (*see*, for example, Fig. 12b). It is not clear whether the observed effects of ${}_tp_1/p_\infty$ are due to compressibility or to change in Reynolds number. The relevant values of the latter are tabulated at the head of Fig. 12.

In view of the results discussed above, the effects of L/d_1 and a_2/a_1 on the outlet profiles were measured at one value of the jet pressure ratio only (${}_tp_1/p_\infty = 2{\cdot}00$). The results obtained with the shrouds of Group 2 ($a_2/a_1 = 1{\cdot}10$) are plotted in Fig. 13 while Figs. 14 and 15 respectively show the corresponding curves for the shrouds of Group 3 ($a_2/a_1 = 1{\cdot}93$) and Group 4 ($a_2/a_1 = 2{\cdot}90$). In each of these three figures the velocity profiles are presented in terms of both u/u_c and u/u^* (*see* 'List of Symbols') for reasons which will become apparent later.

We consider first the upper graph in Fig. 13 and note that as L/d_1 is increased the outlet profiles appear to approach, asymptotically, a limiting profile for which the velocity distribution is nearly uniform over most of the outlet cross-section. In the actual experiment L/d_1 was not increased sufficiently for this limiting (or equilibrium) profile to be attained but it presumably lies slightly above the observed profile for $L/d_1 = 32$.

Now mixing of the primary and secondary streams within the shroud in the present experiment is closely analogous to the development of the boundary layer in a long cylindrical pipe with a faired entry. In both cases the velocity profile at entry is virtually discontinuous and this profile is progressively smoothed out by turbulent mixing. The main difference lies in the number and radial position of the initial discontinuities. In the case of pipe flow there is but one discontinuity, which is located at the wall. With the ejector, on the other hand, there are two discontinuities; one at the wall of the shroud, and one at the lip of the primary nozzle. Intuitively, it seems reasonable to suppose that, provided the shroud (or pipe) is long enough, the form of the velocity profile at exit will not depend on the form of the profile at entry. On these grounds therefore, we would expect the limiting outlet profile in the case of the ejector to be the same as the 'fully-developed turbulent pipe-flow' profile measured by Stanton and Nikuradse[2] for incompressible flow, and by Frössel[3] for compressible flow. Such, however, is not the case.

To check the results of Refs. 2 and 3 a fresh determination was made of the fully-developed turbulent pipe-flow profile. To this end the shroud was removed and a straight cylindrical pipe fifty nozzle diameters in length attached to the primary nozzle. This pipe was traversed across one

radius at axial stations situated 30, 40 and 50 nozzle diameters downstream of the primary nozzle. These traverses were made at jet pressure ratios ($_tp_1/p_\infty$) of 1·25 and 1·65, corresponding to outlet velocities (on the centreline) of about 550 and 850 ft/sec respectively. The six profiles thus obtained were practically identical, indicating that equilibrium had been reached, and the mean of the six profiles, which agreed well with the results of Refs. 2 and 3, is plotted on the upper graph in Fig. 13 as a chain-dotted line. It is immediately apparent that this line will not serve as a limiting curve for the family of ejector profiles. It is true that the Reynolds numbers for the pipe-flow profile ($0{\cdot}5 \times 10^6$ and $0{\cdot}9 \times 10^6$) are slightly lower than that for the ejector profiles ($1{\cdot}2 \times 10^6$) but this difference is far too small to account for the discrepancy. No reasonable explanation of this rather puzzling result has so far been found.

The attenuation in noise produced by an ejector is largely dependent on the velocity distribution at the shroud outlet relative to the outlet velocity of the unshrouded primary nozzle at the same jet pressure ratio. Accordingly, in the lower graph of Fig. 13, the velocity profiles are replotted with u/u^* as ordinate. Two features of these curves are important. Firstly, taking the unshrouded primary nozzle as a datum, the shrouds reduce the maximum transverse gradient of the velocity in the exit plane. This effect is most noticeable with the shorter shrouds. Secondly, there is a progressive decrease in centreline velocity with increase in shroud length. Both these factors have a favourable effect on the noise. We see also that, roughly speaking, the five curves intersect at a common point. The reason will be evident from Fig. 18b which shows the total-pressure distribution (expressed as $_tp-p_\infty/_tp_1-p_\infty$) within a shroud. It is apparent that, to a first approximation, $_tp - p_\infty/_tp_1 - p_\infty$ is constant along any straight line through the primary-nozzle lip in the meridian plane. Moreover, it seems probable that the relation between $_tp - p_\infty/_tp_1 - p_\infty$ and α (defined in Fig. 18b) is independent of shroud length, although this point was not checked experimentally. On this assumption it follows immediately that the parameter $(_tp-p_\infty)/(_tp_1-p_\infty)$ is independent of L/d_1 at the point where $r = r_1$ in the shroud outlet plane (but at no other point in this plane). Since u/u^* depends only on $(_tp-p_\infty)/(_tp_1-p_\infty)$ at a given value of jet pressure ratio, the result observed in Fig. 13 is explained.

The curves for the shrouds of Group 3 ($a_2/a_1 = 1{\cdot}93$) and Group 4 ($a_2/a_1 = 2{\cdot}90$) are presented in Figs. 14 and 15. They are very similar qualitatively to those considered above so that separate discussion is unnecessary. It is, however, instructive to compare the lower graphs in Figs. 13, 14 and 15 with reference to noise even though, in the lack of direct acoustic evidence, the conclusions reached must be regarded as provisional.

It is well known that for given ambient conditions the acoustic power (P) of a subsonic jet is given by,

$$P = K\rho^2 d^2 u^8 \tag{7}$$

where ρ, d and u refer to the nozzle outlet plane and K is a parameter which is practically constant. This formula has been tested experimentally over a wide range and found to be valid provided that the initial velocity profile of the jet is reasonably uniform and the initial turbulence level 'average'. Subject to these restrictions and assuming a representative polar distribution of intensity we can, therefore, readily calculate the sound intensity produced by a jet at any point in the far field. This has been done for the three shrouds which have a reasonably uniform velocity profile ($L/d_1 = 32$). In this calculation the centreline velocity (u_c) was substituted in equation (7). The resulting noise levels are compared with the calculated noise level of the unshrouded primary nozzle in Table 4 below.

TABLE 4

$_tp_1/p_\infty = 2{\cdot}00$. $l/d_1 = 0{\cdot}5$. $L/d_1 = 32$.

$\frac{a_2}{a_1}$	$\frac{u_c}{u^*}$	I (db)	Attenuation (db)
Primary Nozzle	1·000	119	0
1·10	0·738	111	8
1·93	0·658	108	11
2·90	0·606	107	12

Note: I denotes the noise intensity level in decibels (relative to 10^{-16} watts/cm^2) at a point 10 ft from the shroud outlet at an angle of 30° to the jet axis.

If attenuations of this magnitude can be achieved in practice they are clearly very well worthwhile, even allowing for the excessive shroud length. However, the calculations may be in error for three reasons. Firstly, the turbulence level at the shroud outlet is probably appreciably higher than 'average'; secondly, the outlet velocity profiles are not quite uniform; and thirdly, the noise generated downstream of the shroud outlet may be supplemented by radiation through the walls and inlet, and this latter is not included in the calculated values.

6.6. *The Effect of $_tp_1/p_\infty$, L/d_1 and a_2/a_1 on the Thrust Parameter (σ).*

The results of the thrust measurements on the shrouds of Groups 2, 3 and 4 are shown in Fig. 16. To facilitate direct comparison between the thrust of the ejector and that of the unshrouded primary nozzle, the thrust parameter (σ) is taken as ordinate in this figure (*see* 'List of Symbols'). Also shown are the values of σ predicted by the one-dimensional ejector theory of Appendix I.

It will be seen that the experimental curves are similar in form to the corresponding curves for the mass-flow parameter (λ) presented in Figs. 9, 10 and 11. As L/d_1 is increased at a given value of $_tp_1/p_\infty$, σ first increases fairly rapidly, then reaches a peak value, and finally slowly decreases. Conversely, when L/d_1 is constant σ decreases as $_tp_1/p_\infty$ increases. Even at the peaks, the experimental curves lie below the corresponding theoretical curves which, for the reasons given in Section 3, are independent of L/d_1. The experimental values of σ_{max} are compared with the theoretical values (σ_{theo}) in Table 5 below.

TABLE 5

$\frac{a_2}{a_1}$	$\frac{_tp_1}{p_\infty}$	σ_{max}	σ_{theo}	$\frac{\sigma_{max}}{\sigma_{theo}}$	$\left(\frac{L}{d_1}\right)_{\sigma=\sigma_{max}}$
1·10	1·4	1·110	1·171	0·95	9
	2·0	1·067	1·137	0·94	9
1·93	1·4	1·144	1·242	0·92	12
	2·0	1·110	1·193	0·93	14
2·90	1·4	1·188	1·292	0·92	15
	2·0	1·154	1·242	0·93	17

We conclude from this table that for each combination of ${}_tp_1/p_\infty$ and a_2/a_1 the maximum value of σ is 92 to 95 per cent of the theoretical figure. The corresponding values of L/d_1, which depend on both ${}_tp_1/p_\infty$ and a_2/a_1, range from 9 to 17.

However, although this comparison is interesting, the most important practical feature of Fig. 16 and Table 5 is simply the absolute magnitude of σ, which is greater than unity over almost the whole of the operating range. In particular, at a jet pressure ratio of 2·0, σ_{max} ranges from about 1·07 when $a_2/a_1 = 1{\cdot}10$ to about 1·15 when $a_2/a_1 = 2{\cdot}90$. A gain in take-off thrust of this order is clearly highly desirable, especially since it can be achieved with a relatively modest shroud length. Moreover, if the jet pressure ratio is sufficient to choke the unshrouded primary nozzle (${}_tp_1/p_\infty \geqslant 1{\cdot}893$), the engine operating conditions (including the fuel flow) remain precisely the same whether a shroud is present or not. Under these conditions, therefore, the ratio

$$\frac{\text{Specific Fuel Consumption with Ejector}}{\text{Specific Fuel Consumption with unshrouded Primary Nozzle}} \text{ is equal to } \frac{1}{\sigma}.$$

It is also instructive to compare the measured values of σ shown in Fig. 16 with the calculated noise intensity levels given in Table 4. This comparison is only possible for the longest shrouds ($L/d_1 = 32$) at a jet pressure ratio of 2·0. The relevant data are given in Table 6 below.

TABLE 6

${}_tp_1/p_\infty = 2{\cdot}00.\quad l/d_1 = 0{\cdot}5.\quad L/d_1 = 32.$

$\frac{a_2}{a_1}$	Attenuation db (re-unshrouded primary nozzle)	Thrust (re-unshrouded primary nozzle)
1·10	8	0·96
1·93	11	1·02
2·90	12	1·09

The calculated attenuation levels may be in error for the reasons given in Section 6.5. If we accept them, however, it is apparent that a shroud can both reduce the noise level and increase the thrust relative to the basic propelling nozzle. Against these advantages we must offset the weight penalty and installational difficulties.

6.7. *The Effect of ${}_tp_1/p_\infty$ on the Distribution of Static Pressure along the Shroud Wall.*

The distribution of static pressure along the shroud wall was measured for two of the shrouds of Group 2 ($L/d_1 = 12$ and 32) at jet pressure ratios ranging from 1·0 to 2·0. Fig. 17a and b shows the results.

In both these graphs we note a small irregularity in the curves at the point $x/L = 0$. The reasons for this are as follows. Owing to the finite thickness of the primary-nozzle wall there is a slight increase in the cross-sectional area of the subsonic secondary flow at the primary-nozzle lip, and hence an increase in the static pressure of the secondary stream. This is the sole cause of the irregularity provided that the primary flow is subsonic (${}_tp_1/p_\infty < 1{\cdot}65$). If, however, ${}_tp_1/p_\infty > 1{\cdot}65$ the primary nozzle is choked. The primary stream then expands downstream of the nozzle outlet and therefore the secondary stream contracts. Consequently, after the initial rise due to lip thickness, the wall pressure decreases. This is clearly visible in Fig. 17a and b.

Discounting this effect we see that in Fig. 17a, the wall pressure increases continuously over the entire length of the shroud. In Fig. 17b, however, the wall pressure first rises to a value greater than p_∞ and then drops almost uniformly to p_∞ at the shroud outlet. This difference is a measure of the extent to which mixing is complete in the two shrouds. When $L/d_1 = 12$ mixing is incomplete even at the shroud outlet (*see* Fig. 13). However, when $L/d_1 = 32$ mixing is practically complete at the shroud outlet (*see* Fig. 13), and there is probably very little change in the velocity profile for some distance upstream of the outlet. In this case, therefore, skin friction causes the wall pressure to decrease over the latter part of the shroud, as shown in Fig. 17b.

6.8. *The Development of the Mixing Process within the Shroud.*

One shroud (Group 2, $L/d_1 = 12$) was chosen for a more detailed study of the mixing process between the primary and secondary streams. At a jet pressure ratio of 1·65, pitot-and static-pressure profiles were measured across one radius at seven equally spaced axial stations. The terminal stations were situated at the outlet plane of the primary nozzle and the outlet plane of the shroud respectively.

It was found, firstly, that at each axial station the static pressure at any point in the flow did not differ from the wall pressure by more than one per cent. The variation in wall pressure along the shroud is shown in Fig. 18a.

The total-pressure profiles are shown in Fig. 18b. In this figure the parameter $({}_tp - p_\infty)/({}_tp_1 - p_\infty)$ is taken as ordinate. This parameter is most appropriate for the present purpose because, prior to mixing, it is equal to unity in the free primary stream and zero in the free secondary stream. It therefore normalises the graph and makes the boundaries of the mixing region readily apparent.

The most obvious feature of Fig. 18b is the progressive decrease in total pressure of the primary stream and increase in total pressure of the secondary stream which results from the continual transfer of momentum and energy across the interface. This process is, of course, one of the most general characteristics of a mixing region, either turbulent or laminar. By its action the virtual discontinuity in total pressure at the primary-nozzle lip is progressively smoothed out, until at a sufficient distance downstream the profile becomes practically independent of axial position. In the present instance, however, the shroud is not long enough for this state of equilibrium to be attained, mixing being still incomplete at the shroud outlet (*see* also Fig. 13).

Fig. 18b shows also the variation in total pressure along straight lines drawn through the primary-nozzle lip in the meridian plane. As mentioned previously (Section 6.5) it will be seen that the total pressure is nearly constant along any such line. To this extent the present example of a mixing process resembles the simplest possible example; namely, mixing at the boundary of a subsonic two-dimensional half-jet discharging into an infinite static atmosphere[4]. In the latter case, however, the static pressure also is constant along the lines in question. This is not true of the ejector (*see* Fig. 18a). We note finally, from the lines of constant α in Fig. 18b, that the boundaries of the mixing region subtend an angle of about 7° at the primary-nozzle lip. The corresponding angle for the analogous case cited above is about 12°.

7. *Subjective Observations on the Noise.*

No objective measurements of the noise were made during these tests. Nevertheless, certain subjective observations on the acoustic characteristics of the ejectors deserve comment. As a general rule the ejectors made a loud roar of indeterminate pitch. This is the normal effect on the ear of the

continuous frequency spectrum associated with jet noise. Aurally it was not possible to arrange the shrouds in order of loudness or even to compare them with the unshrouded primary nozzle. The reasons lay partly in the relatively long time interval between successive tests and partly in the high level of background noise. The latter, which was caused by control bleeds, plant and reflections within the laboratory, tended to mask the jet noise.

The acoustic properties of three of the shrouds were abnormal. The shrouds in question were the shortest members of Groups 2, 3 and 4 ($L/d_1 = 3$). In addition to the normal jet roar these emitted an intense discrete-frequency noise. A definite pitch could always be assigned to this sound, but it was not a pure tone (i.e., it consisted of a fundamental and harmonics). The three shrouds behaved differently as regards the effect of jet pressure ratio on this discrete-frequency noise. With the Group 4 shroud the intensity increased continuously as the jet pressure ratio increased but the pitch remained constant. Increasing the jet pressure ratio with the Group 3 shroud resulted in a continuous increase in intensity but the pitch rose discontinuously, presumably from one harmonic to a higher harmonic. Under some conditions two notes would sound together. The Group 2 shroud behaved in a similar manner to the Group 3 shroud as regards pitch but in this case the sound almost vanished as soon as the primary nozzle choked.

The evidence on pitch indicates very strongly that the discrete-frequency noise is caused by 'organ pipe' resonance. By this we mean that stationary waves are set up such that the vibrations at each point in the shroud are in phase and of the same frequency. This frequency depends on the shroud length and the mode of vibration.

Resonance is presumably excited and maintained by instability of the flow. In the case of two of the shrouds (Groups 3 and 4) the irregular variation in M_2 with ${}_tp_1/p_\infty$ (Fig. 8b and c) provides additional evidence of this instability (*see* also Section 6.4). As regards the Group 2 shroud, however, the evidence for instability rests on the discrete-frequency noise only, since the M_2 curve was normal.

Discrete-frequency noise is primarily an acoustic phenomenon and, as such, lies outside the terms of reference of the experiment. Moreover, in the present instance, the shrouds concerned were too short to be of much practical interest. The matter was not, therefore, investigated in detail. Nevertheless, it is possible that on a larger scale and at a higher jet pressure ratio, instability and resonance may occur with longer shrouds. One cannot, therefore, feel entirely confident about the practical application of ejectors to noise suppression until this point has been investigated more thoroughly.

8. *Conclusions.*

The main conclusions drawn from the experimental work may be summarised thus:

(i) When a convergent nozzle discharges into a cylindrical shroud the primary flow from the nozzle entrains from the atmosphere a secondary flow. This secondary flow is accelerated through the shroud entry to a velocity which is less than the primary-jet velocity. Consequently there exists a discontinuity in the velocity profile across the shroud in the primary-nozzle exit plane. Downstream of this plane turbulent mixing of the primary and secondary streams tends to smooth out the discontinuity. If the shroud is relatively short the velocity profile at the exit is non-uniform. The centreline velocity differs but little from that of the unshrouded primary nozzle but the maximum transverse velocity gradient is reduced. As the shroud length is increased the outlet profile tends to a limiting form with a velocity distribution which is nearly constant over the

cross-section. With a long shroud, therefore, the velocity at exit is practically uniform and appreciably less than that of the unshrouded primary nozzle. These characteristics of the mixing process affect both the thrust and the noise level of the system.

(ii) To achieve complete mixing a shroud length of about 30 times the primary-nozzle diameter ($L/d_1 = 30$) is required. The following table shows comparative figures for the thrust and centreline exit velocity with complete mixing. The tabulated values apply to the longest shrouds tested ($L/d_1 = 32$) at a jet pressure ratio of 2·0.

$\frac{a_2}{a_1}$	Thrust (re-unshrouded primary nozzle)	Centreline exit velocity (re-unshrouded primary nozzle)
1·10	0·96	0·74
1·93	1·02	0·66
2·90	1·09	0·61

(iii) Even with comparatively short shrouds ($L/d_1 = 5$) a thrust ratio of 1·05 is obtained at a jet pressure ratio of 2·0. With these shrouds the reduction in centreline velocity at the exit is insignificant but the maximum transverse gradient of velocity is decreased.

(iv) At a jet pressure ratio of 2·0 the maximum measured value of the thrust ratio was 1·15. This value was obtained with an ejector area ratio (a_2/a_1) of 2·90 and a shroud length (L/d_1) of 17.

(v) In addition to the normal jet roar, the three shortest shrouds ($L/d_1 = 3$) emit an intense discrete-frequency noise. This is probably caused by instability of the flow in the mixing region which excites 'organ pipe' resonance in the shroud.

9. *Acknowledgment.*

The author wishes to thank Mr. J. C. Davies for his assistance with the experimental work.

LIST OF SYMBOLS AND DEFINITIONS

The notation is shown, in part, in Fig. 1.

Suffixes.

$(\ )_1$ $(\ )_2$ and $(\ )_3$ refer to the positions shown in Fig. 1.

$(\ )_\infty$ refers to the ambient static atmosphere

$(\ )_c$ denotes a value on the axis of symmetry

$(\ )_w$ denotes a value on the shroud wall

$_t(\ )$ refers to stagnation conditions

Flow Parameters.

M	Mach number
u	Velocity
ρ	Density
p	Static pressure
T	Static temperature
Q	Rate of mass flow
γ	Ratio of specific heats
R	Gas constant
Re	Reynolds number (based on shroud diameter and mean conditions in shroud exit plane)

Geometrical Parameters.

r	Radial distance from axis, or (with a suffix) radius of duct
d	Diameter
a	Cross-sectional area
x	Axial distance from primary-nozzle exit plane
l	Approach length } *see* Fig. 1
L	Mixing length } *see* Fig. 1

Miscellaneous Definitions.

The mass-flow parameter (λ) is defined by the equation:

$$\lambda = \frac{Q_2}{Q_1}\frac{a_1}{a_2}\sqrt{\frac{{}_tT_2}{{}_tT_1}}$$ (*see* Appendix II).

The thrust parameter (σ) is defined by the equation:

$$\sigma = \frac{S}{S_0}$$

where S denotes the thrust of a given ejector system and S_0 denotes the thrust of the unshrouded primary nozzle operating at the same values of ${}_tp_1$ and p_∞ (*see* Appendix II).

u^* denotes the velocity corresponding to isentropic expansion at ${}_tT_1$ through pressure ratio ${}_tp_1/p_\infty$.

Nomenclature.

${}_tp_1/p_\infty$	Jet pressure ratio
${}_tT_2/T_1$	Jet temperature ratio
a_2/a_1	Ejector area ratio
L/d_1	Mixing-length ratio
l/d_1	Approach-length ratio

REFERENCES

No.	*Author(s)*	*Title, etc.*
1	J. Reid and R. C. Hastings ..	Experiments on the axi-symmetric flow over afterbodies and bases at $M = 2{\cdot}0$. A.R.C. 21,707. October, 1959.
2	S. Goldstein (editor)	*Modern developments in fluid dynamics.* Vol. II. Chapter 8. Section 3. Clarendon Press, Oxford. 1938.
3	W. Frössel	Flow in smooth straight pipes at velocities above and below sound velocity. N.A.C.A. Tech. Memo. 844. A.R.C. 5602. January, 1942.
4	H. W. Liepmann and J. Laufer ..	Investigations of free turbulent mixing. N.A.C.A. Tech. Note 1257. August, 1947.

APPENDIX I

One-Dimensional Ejector Theory

Note. The notation corresponds to that of Fig. 1 and the 'List of Symbols'.

Consider an ejector system consisting of an axisymmetric convergent primary nozzle surrounded by a cylindrical shroud with a convergent secondary air entry (Fig. 1). The ambient air is static and we make the following assumptions.

1. $d_0 = d_1$.
2. ${}_tp_2 = p_\infty$.
3. Uniform flow at planes [1] and [2].
4. ${}_tT_1 = {}_tT_2$.
5. Uniform flow at plane [3].
6. No skin friction.

The relevant equations are then:

Continuity

$$\rho_1 u_1 a_1 + \rho_2 u_2 a_2 = \rho_3 u_3 (a_1 + a_2). \tag{8}$$

Momentum

$$(p_1 + \rho_1 u_1^2) a_1 + (p_2 + \rho_2 u_2^2) a_2 = (p_3 + \rho_3 u_3^2)(a_1 + a_2) \tag{9}$$

Energy

$${}_tT_1 = {}_tT_2 = {}_tT_3. \tag{10}$$

Expressed in terms of non-dimensional quantities equations (8) and (10) reduce to:

$$M_1 \sqrt{\left(1 + \frac{\gamma - 1}{2} M_1^2\right)} + \frac{a_2}{a_1}\frac{p_2}{p_1} M_2 \sqrt{\left(1 + \frac{\gamma - 1}{2} M_2^2\right)} = \left(1 + \frac{a_2}{a_1}\right)\frac{p_3}{p_1} M_3 \sqrt{\left(1 + \frac{\gamma - 1}{2} M_3^2\right)} \tag{11}$$

and equation (9) reduces to:

$$(1 + \gamma M_1^2) + \frac{a_2}{a_1}\frac{p_2}{p_1}(1 + \gamma M_2^2) = \left(1 + \frac{a_2}{a_1}\right)\frac{p_3}{p_1}(1 + \gamma M_3^2). \tag{12}$$

It follows immediately from equations (11) and (12) that:

Theorem

If any pair of the three quantities M_1, M_2 and M_3 is equal to unity, then so is the third.

Now any set of parameters corresponding to a real flow must satisfy equations (11) and (12) [and hence the theorem] together with the following conditions.

(i) $M_1 \leqslant 1$. $M_2 \leqslant 1$. $M_3 \leqslant 1$ (because of the geometry of the system).

(ii) $M_2 \leqslant M_1$ (because ${}_tT_2 = {}_tT_1$ and it is clear physically that $u_2 \leqslant u_1$).

(iii) If $M_1 < 1$ and $M_2 < 1$ then $p_2/p_1 = 1$.

(iv) If $M_3 < 1$ then $p_3/p_\infty = 1$ and if $M_3 = 1$ then $p_3/p_\infty \geqslant 1$.

Of the eight possible combinations of M_1, M_2 and M_3 implied by condition (i), two are ruled out by the theorem, two more are eliminated by condition (ii) and a fifth is incompatible with condition (iv). There are left only three cases which are physically real. These are:

I $M_1 < 1$, $M_2 < 1$, $M_3 < 1$, in which case $p_2/p_1 = 1$ and $p_3/p_\infty = 1$.

II $M_1 = 1$, $M_2 < 1$, $M_3 < 1$, in which case $p_3/p_\infty = 1$.

and

III $M_1 = 1$, $M_2 = 1$, $M_3 = 1$.

We will now consider these three cases in more detail.

Case I

($M_1 < 1$, $M_2 < 1$, $M_3 < 1$, $p_2/p_1 = 1$, $p_3/p_\infty = 1$)

Equations (11) and (12) then become:

$$M_1\sqrt{\left(1+\frac{\gamma-1}{2}M_1^2\right)}+\frac{a_2}{a_1}M_2\sqrt{\left(1+\frac{\gamma-1}{2}M_2^2\right)}=\left(1+\frac{a_2}{a_1}\right)\frac{{}_\iota p_2}{p_2}M_3\sqrt{\left(1+\frac{\gamma-1}{2}M_3^2\right)} \tag{13}$$

$$(1+\gamma M_1^2)+\frac{a_2}{a_1}(1+\gamma M_2^2)=\left(1+\frac{a_2}{a_1}\right)\frac{{}_\iota p_2}{p_2}(1+\gamma M_3^2). \tag{14}$$

We have also the isentropic relations:

$$\frac{{}_\iota p_1}{p_1}=f(M_1) \tag{15}$$

$$\frac{{}_\iota p_2}{p_2}=f(M_2) \tag{16}$$

and, finally

$$\frac{{}_\iota p_1}{p_\infty}=\frac{{}_\iota p_1}{p_1}\frac{p_2}{{}_\iota p_2}. \tag{17}$$

From these 5 equations we can eliminate any 4 of the 7 variables (M_1, M_2, M_3, ${}_\iota p_1/p_1$, ${}_\iota p_2/p_2$, ${}_\iota p_1/p_\infty$ and a_2/a_1) and hence express M_1, M_2 and M_3, together with the derived parameters λ and σ (*see* Appendix II), in terms of ${}_\iota p_1/p_\infty$ and a_2/a_1. The problem is therefore solved in principle, and although it is not convenient to obtain explicit formulae, the numerical calculation is not too difficult.

A special case of some interest which is soluble explicitly arises when ${}_\iota p_1/p_\infty$ is nearly equal to unity (incompressible flow). Making the usual approximations in equations (13) to (17) and in equations (33) and (39) of Appendix II we then find that:

$$\lambda=\frac{-2\frac{a_2}{a_1}+\left(1+\frac{a_2}{a_1}\right)\sqrt{\left(2\frac{a_2}{a_1}\right)}}{1+\left(\frac{a_2}{a_1}\right)^2} \tag{18}$$

and

$$\sigma=\frac{\left(1+\lambda\frac{a_2}{a_1}\right)^2}{\left(1+\frac{a_2}{a_1}\right)(1-\lambda^2)}. \tag{19}$$

In this case, therefore, the unknowns (p_2/p_1 and p_3/p_∞) can be expressed as explicit functions of ${}_\iota p_1/p_\infty$ and a_2/a_1 and the problem is thus solved. It is of interest that, under these conditions, the mass-flow parameter is given by the simple relation

$$\lambda = \frac{1}{{}_\iota p_1/p_\infty} \tag{30}$$

and is therefore independent of a_2/a_1.

λ and σ are plotted as functions of ${}_\iota p_1/p_\infty$ and a_2/a_1 in Figs. 2 and 3 respectively.

APPENDIX II

The Mass-Flow Parameter (λ) *and the Thrust Parameter* (σ)

I. *The Mass-Flow Parameter.*

Consider first the flow through the primary nozzle. It is assumed that:

(i) The flow is axisymmetric.

(ii) The total temperature is constant everywhere.

$(\ )_1$ denotes conditions just outside the boundary layer in plane [1], (Fig. 1).

Then it is easily shown by integration that:

$$\frac{Q_1\sqrt{{}_tT_1}}{a_1\,{}_tp_1}\sqrt{\frac{R}{\gamma}} = 2\int_0^1 \frac{p}{{}_tp_1} M \sqrt{\left(1+\frac{\gamma-1}{2}M^2\right)}\ \zeta\, d\zeta \tag{31}$$

where

$$\zeta = \frac{r}{r_1}.$$

Equation (31) may be re-written

$$\frac{Q_1\sqrt{{}_tT_1}}{a_1\,{}_tp_1}\sqrt{\frac{R}{\gamma}} = C_{D1}\frac{p_1}{{}_tp_1} M_1 \sqrt{\left(1+\frac{\gamma-1}{2}M_1^2\right)} \tag{32}$$

where

$$C_{D1} = 2\int_0^1 \frac{\rho}{\rho_1}\frac{u}{u_1}\,\zeta\, d\zeta.$$

In this equation (32) we note that:

(i) Assuming that the static pressure is constant across the boundary layer, p_1 equals the measured static pressure at the wall (*see* Fig. 4).

(ii) Assuming that the total pressure is constant in the free stream, ${}_tp_1$ equals the measured total pressure upstream of the nozzle (*see* Fig. 4).

(iii) M_1 is related to $p_1/{}_tp_1$ by the usual equation for isentropic flow.

In general, C_{D1} varies with the mass flow through the nozzle, but there are two special cases of interest.

(i) If the flow is uniform across the section then $C_{D1} = 1$.

(ii) If ρ/ρ_1 and u/u_1 are invariant functions of ζ (with respect to the mass flow through the nozzle) then C_{D1} is constant.

Now when suffix 1 is replaced by suffix 2 and $\zeta = r/r_1$ is replaced by $\xi = \sqrt{\{(r^2-r_0^2)/(r_3^2-r_0^2)\}}$, an analogous set of formulae hold for the secondary flow annulus.

The mass-flow parameter is therefore given by

$$\lambda = \frac{Q_2}{Q_1}\frac{a_1}{a_2}\sqrt{\frac{{}_tT_2}{{}_tT_1}} = \frac{C_{D2}}{C_{D1}}\frac{p_2}{p_1}\frac{M_2\sqrt{\left(1+\frac{\gamma-1}{2}M_2^2\right)}}{M_1\sqrt{\left(1+\frac{\gamma-1}{2}M_1^2\right)}} \tag{33}$$

and we may draw the following conclusions with regard to the discharge coefficients C_{D1} and C_{D2}.

(i) In general both C_{D1} and C_{D2} vary with the applied pressure ratio $({}_tp_1/p_\infty)$.

(ii) If the flow is uniform across both the primary and secondary cross-sections, then $C_{D1} = C_{D2} = 1$.

(iii) If the density and velocity profiles across both sections are invariant with respect to the applied pressure ratio $({}_tp_1/p_\infty)$ then C_{D1} and C_{D2} are constant (but not necessarily equal to unity).

II. *The Thrust Parameter.*

Consider a nozzle-shroud combination of given geometry operating at given values of ${}_tp_1$ and p_∞ (Fig. 1).

In general we define the thrust (S) of the system by the equation:

$$S = \int\int^{a_3} (p + \rho u^2) da_3 - p_\infty a_3 . \tag{34}$$

It is easily shown by the momentum theorem that S, defined in this way, is equal to the resultant axial force on the complete engine nacelle at zero flight speed.

Assuming axial symmetry, equation (34) reduces to the more convenient form:

$$\frac{S}{a_3 p_\infty} = 2\int_0^1 \frac{p}{p_\infty}(1+\gamma M^2)\eta\, d\eta - 1 \tag{35}$$

where $\eta = r/r_3$ and the integral is evaluated across plane [3] (Fig. 1).

The reference thrust (S_0) is defined as the thrust of the primary nozzle, with the shroud removed, operating at the same values of ${}_tp_1$ and p_∞ so that, by analogy,

$$S_0 = \int\int^{a_1} (p + \rho u^2) da_1 - p_\infty a_1 \tag{36}$$

which, with axial symmetry, becomes:

$$\frac{S_0}{a_1 p_\infty} = 2\int_0^1 \frac{p}{p_\infty}(1+\gamma M^2)\zeta\, d\zeta - 1 \tag{37}$$

where $\zeta = r/r_1$ and the integral is evaluated across plane [1] (Fig. 1) with the shroud removed.

The thrust parameter (σ) is defined by:

$$\sigma = \frac{S}{S_0}. \tag{38}$$

A special case of particular interest occurs when the flow is one-dimensional in the primary nozzle and at the shroud exit. Equations (35), (37) and (38) combined then reduce to the simple expression

$$\sigma = \frac{S}{S_0} = \frac{a_3}{a_1}\left[\frac{\frac{p_3}{p_\infty}(1+\gamma M_3^2) - 1}{\frac{p_1}{p_\infty}(1+\gamma M_1^2) - 1}\right]. \tag{39}$$

(Note that p_1 and M_1 are evaluated without the shroud).

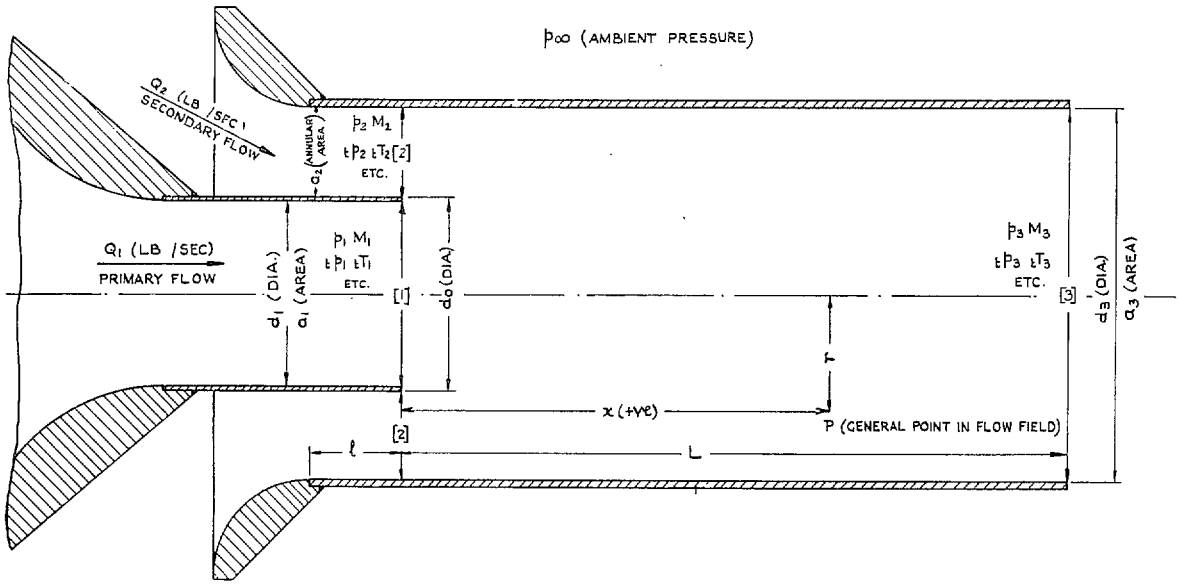

FIG. 1. Diagram showing notation.

NOTE :-

AT POINTS MARKED ⊙ THE PRIMARY NOZZLE IS JUST CHOKED $\left(M_1 = 1,\ \frac{p_2}{p_1} = 1\right)$.

AT POINTS MARKED ⊡ THE SHROUD OUTLET IS JUST CHOKED $\left(M_3 = 1,\ \frac{p_3}{p_\infty} = 1\right)$.

$\frac{t_{T_2}}{t_{T_1}} = 1{\cdot}0$

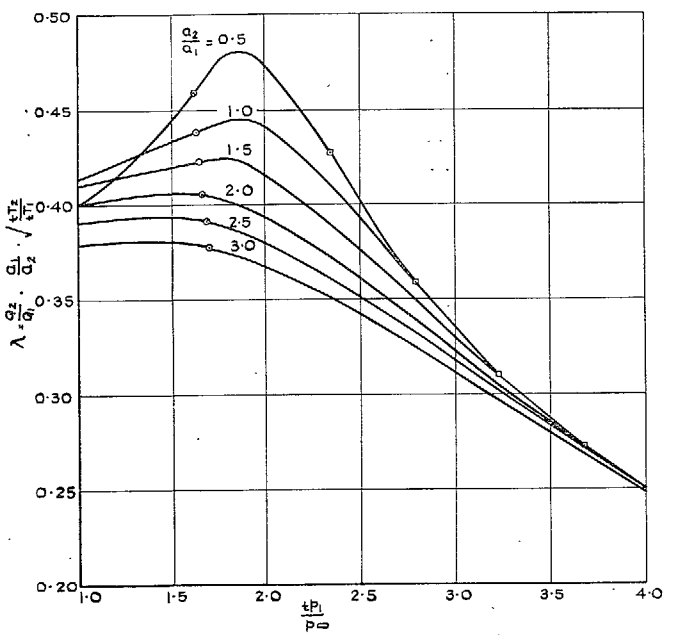

FIG. 2. One-dimensional ejector theory. The mass-flow parameter as a function of the jet pressure ratio and ejector area ratio.

AT POINTS MARKED ⊙ THE PRIMARY NOZZLE IS JUST CHOKED $\left(M_1 = 1,\ \frac{p_2}{p_1} = 1\right)$.

AT POINTS MARKED ⊡ THE SHROUD OUTLET IS JUST CHOKED $\left(M_3 = 1,\ \frac{p_3}{p_\infty} = 1\right)$.

$\frac{t_{T_2}}{t_{T_1}} = 1{\cdot}0$

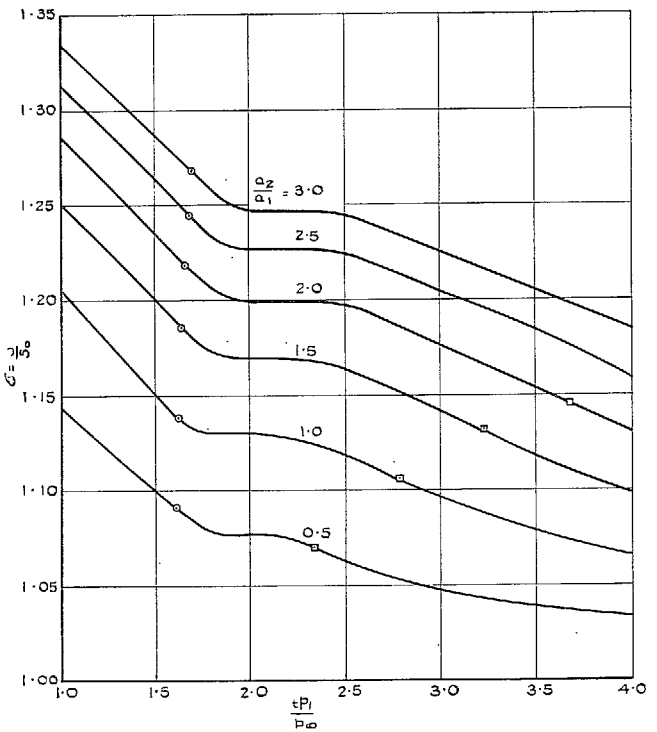

FIG. 3. One-dimensional ejector theory. The thrust parameter as a function of the jet pressure ratio and ejector area ratio.

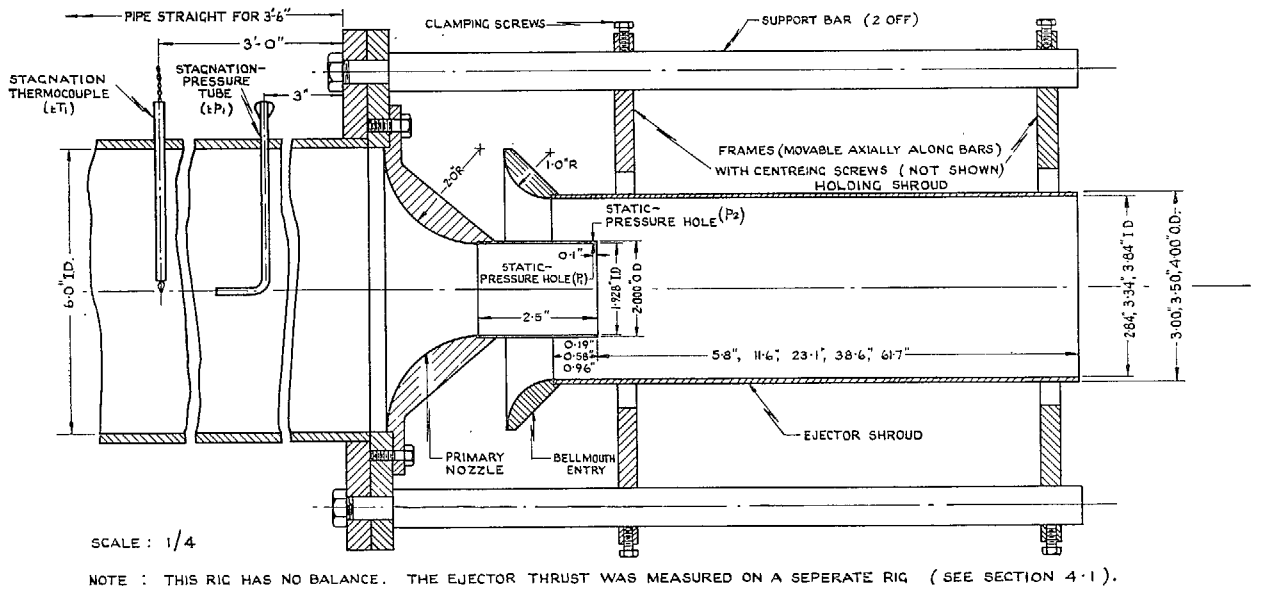

FIG. 4. The experimental rig.

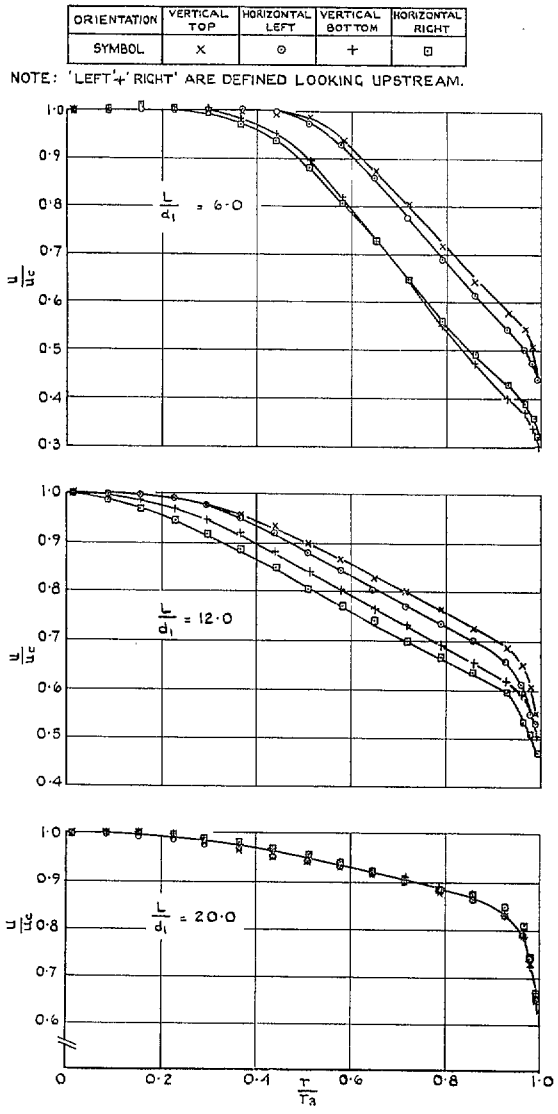

FIG. 5. The effect of mixing-length ratio on the asymmetry of the velocity profiles at the shroud outlet.

$$Re = 1{\cdot}2 \times 10^6, \quad \frac{l}{d_1} = 0{\cdot}5, \quad \frac{a_2}{a_1} = 1{\cdot}10,$$

$$\frac{{}_{t}p_1}{p_\infty} = 2{\cdot}00, \quad \frac{{}_{t}T_2}{{}_{t}T_1} = 1{\cdot}0$$

ℓ/d_1	0·1	0·3	0·5
SYMBOL	×	⊙	+

$\frac{L}{d_1} = 6{\cdot}0$ $\quad \frac{a_2}{a_1} = 1{\cdot}10$ $\quad \frac{t_{T_2}}{t_{T_1}} = 1{\cdot}0$

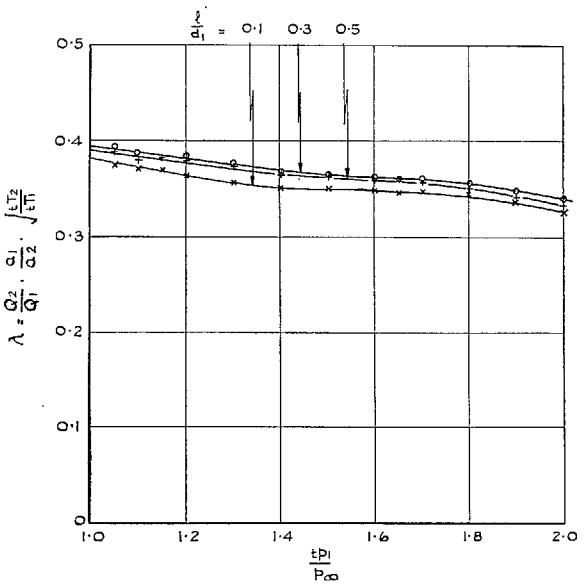

FIG. 6. The effect of approach-length ratio on the variation in mass-flow parameter with jet pressure ratio.

t/d_1	0·1	0·3	0·5
SYMBOL	×	⊙	+

Re = 1·0 × 10⁶

$\frac{L}{d_1} = 6{\cdot}0$ $\quad \frac{a_2}{a_1} = 1{\cdot}10$ $\quad \frac{t_{P_1}}{P_\infty} = 1{\cdot}65$ $\quad \frac{t_{T_2}}{t_{T_1}} = 1{\cdot}0$

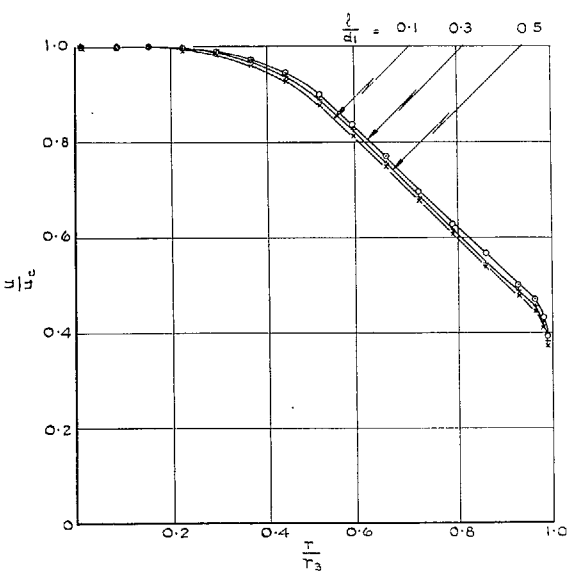

FIG. 7. The effect of approach-length ratio on the velocity profile at the shroud outlet.

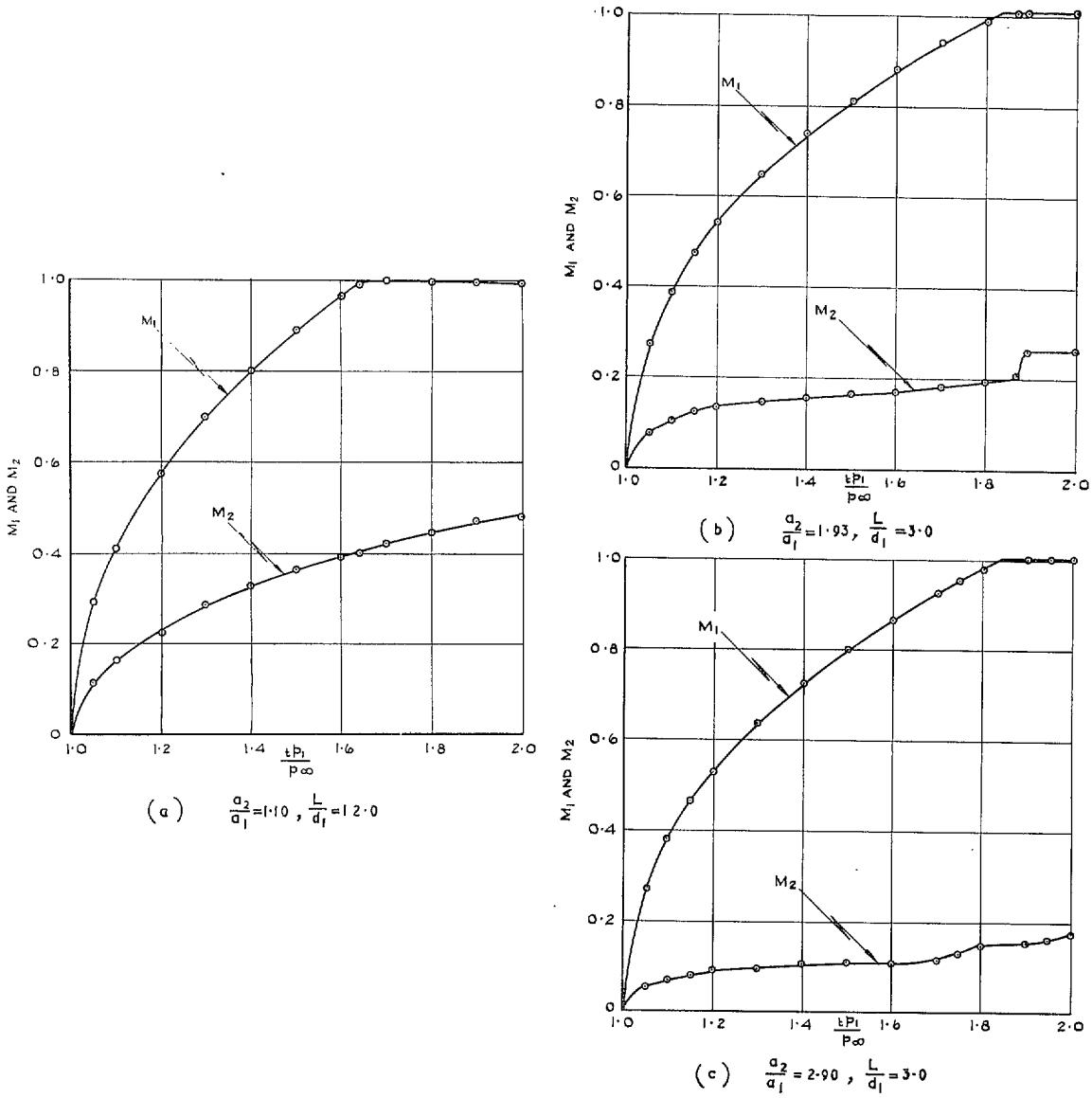

FIG. 8a, b and c. The effect of jet pressure ratio on the Mach number of the primary and secondary flow.

$$\frac{l}{d_1} = 0{\cdot}5, \frac{{}_tT_2}{{}_tT_1} = 1{\cdot}0$$

t_{P_1}/p_∞	1·2	1·4	1·6	1·8	2·0
SYMBOL	×	⊙	+	⊡	◇

FULL LINES DENOTE EXPERIMENTAL RESULTS.

DOTTED LINES DENOTE THEORETICAL RESULTS.

$\frac{l}{d_1} = 0{\cdot}5 \qquad \frac{a_2}{a_1} = 1{\cdot}10 \qquad \frac{t_{T_2}}{t_{T_1}} = 1{\cdot}0$

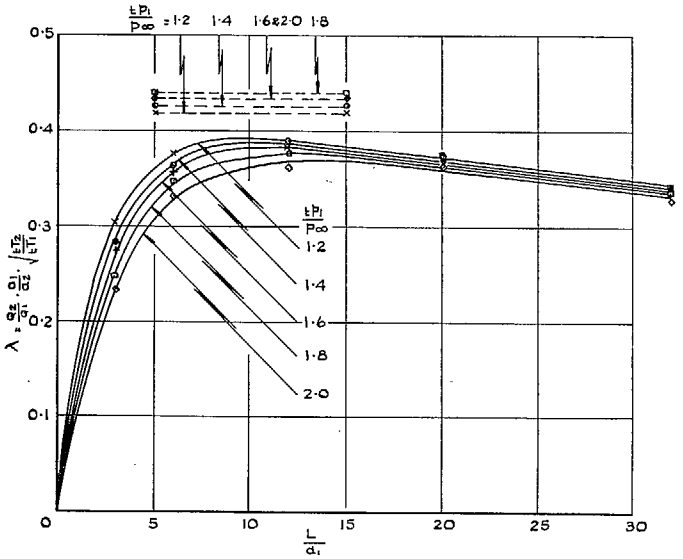

FIG. 9. The effect of mixing-length ratio and jet pressure ratio on the mass-flow parameter.

$a_2/a_1 = 1{\cdot}10$

t_{P_1}/p_∞	1·2	1·4	1·6	1·8	2·0
SYMBOL	×	⊙	+	⊡	◇

FULL LINES DENOTE EXPERIMENTAL RESULTS.

DOTTED LINES DENOTE THEORETICAL RESULTS.

$\frac{l}{d_1} = 0{\cdot}5 \qquad \frac{a_2}{a_1} = 1{\cdot}93 \qquad \frac{t_{T_2}}{t_{T_1}} = 1{\cdot}0$

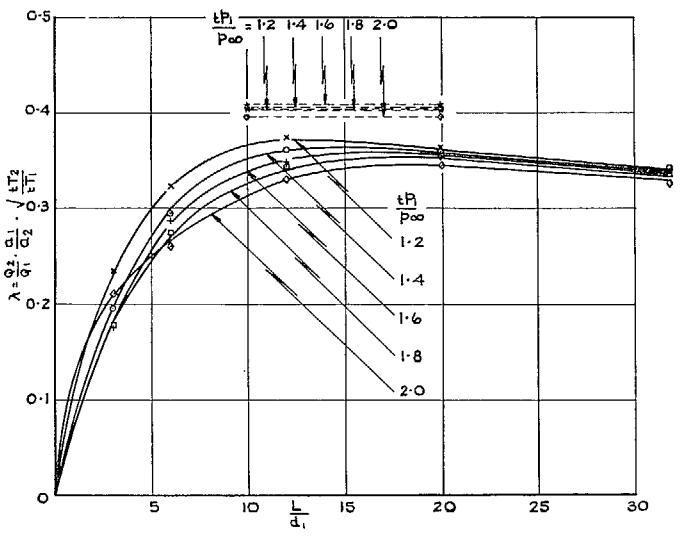

FIG. 10. The effect of mixing-length ratio and jet pressure ratio on the mass-flow parameter.

$a_2/a_1 = 1{\cdot}93$

$t p_1/p_\infty$	1·2	1·4	1·6	1·8	2·0
SYMBOL	×	○	+	□	◇

FULL LINES DENOTE EXPERIMENTAL RESULTS.

DOTTED LINES DENOTE THEORETICAL RESULTS.

$\frac{l}{d_1} = 0{\cdot}5 \qquad \frac{a_2}{a_1} = 2{\cdot}90 \qquad \frac{tT_2}{tT_1} = 1{\cdot}0$

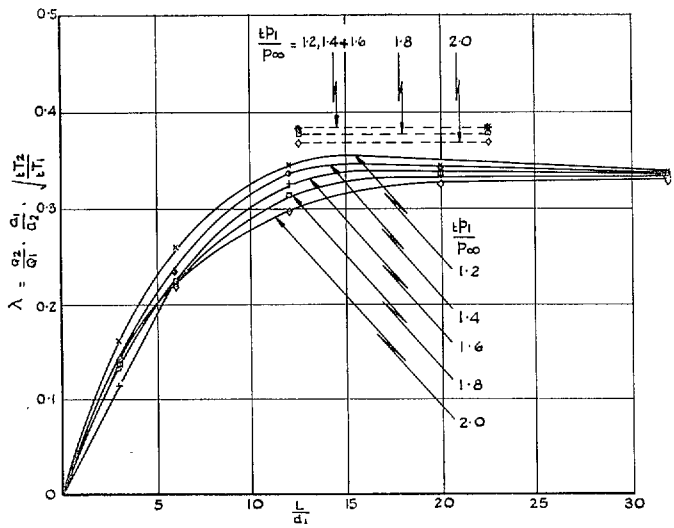

FIG. 11. The effect of mixing-length ratio and jet pressure ratio on the mass-flow parameter.

$a_2/a_1 = 2{\cdot}90$

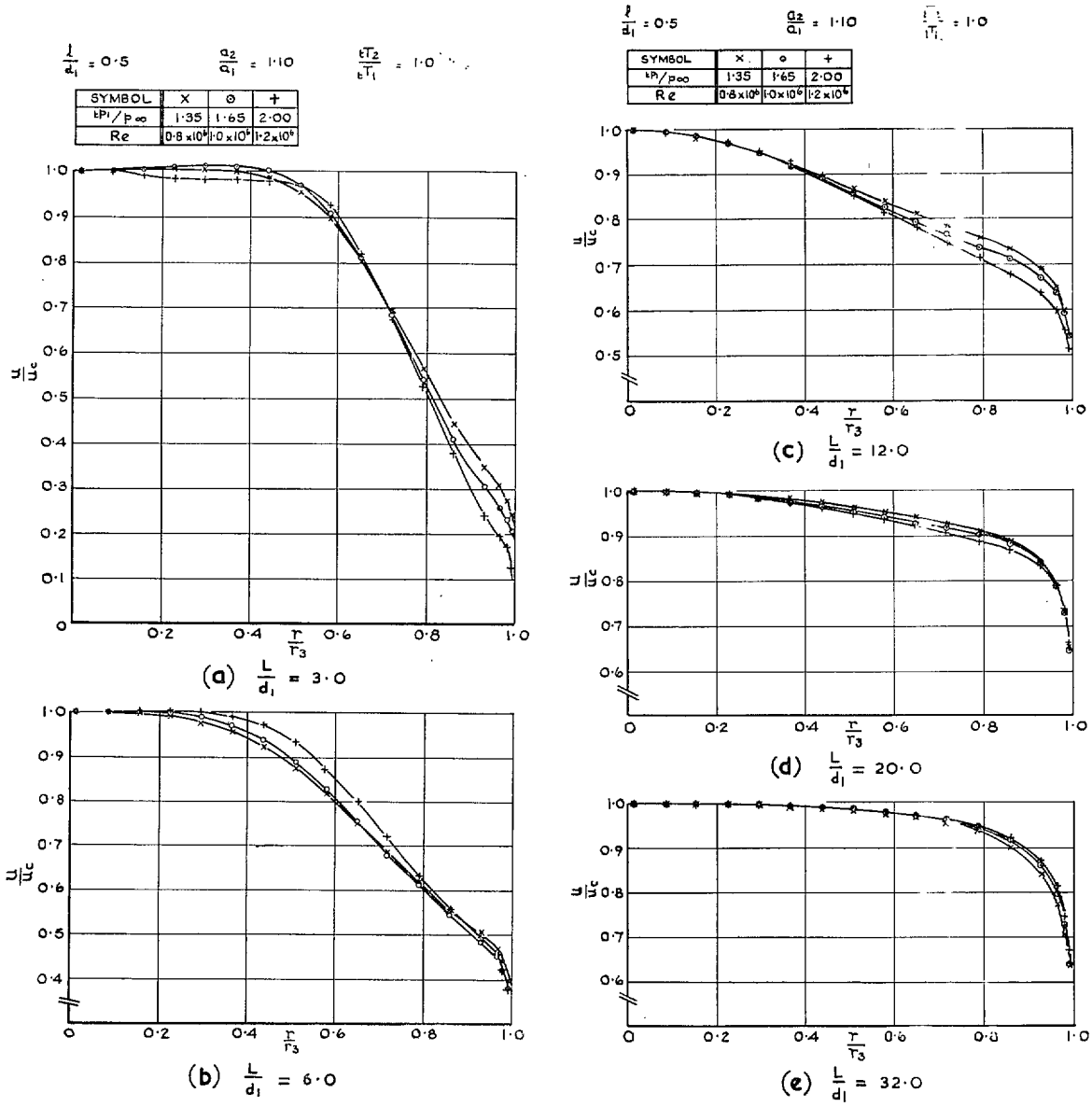

FIG. 12a, b, c, d and e. The effect of jet pressure ratio on the velocity profile at the shroud outlet.

$$\frac{l}{d_1} = 0{\cdot}5, \frac{a_2}{a_1} = 1{\cdot}10, \frac{{}_tT_2}{{}_tT_1} = 1{\cdot}0$$

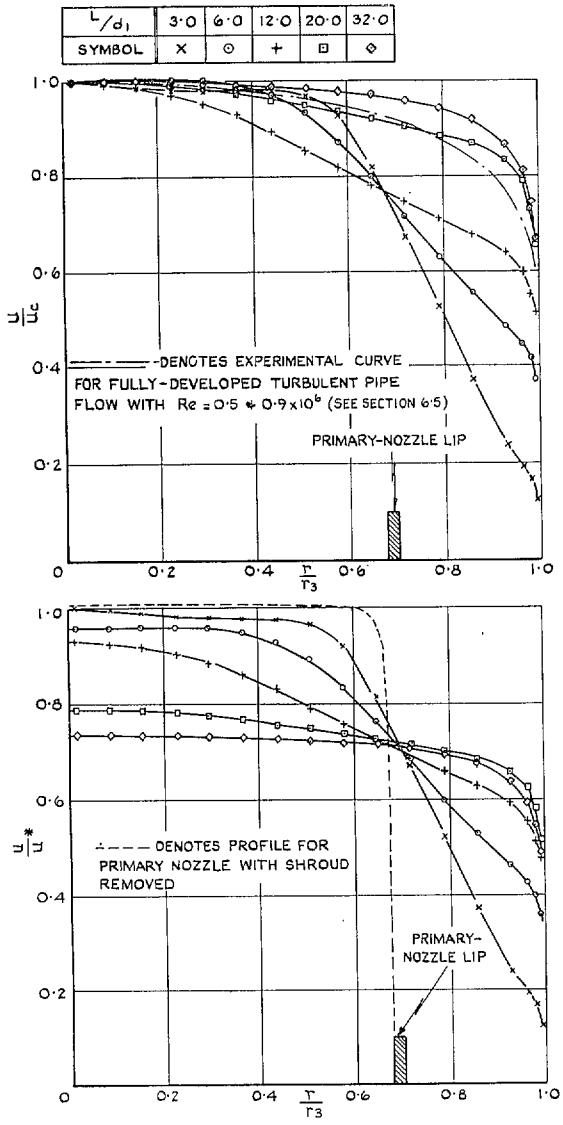

FIG. 13. $\frac{a_2}{a_1} = 1{\cdot}10$

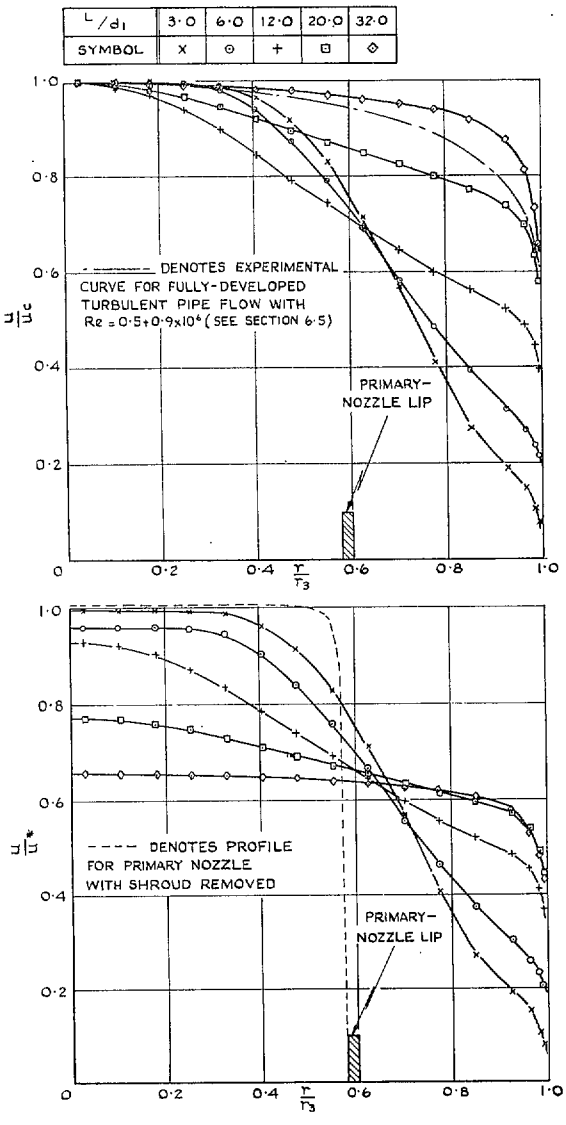

FIG. 14. $\frac{a_2}{a_1} = 1{\cdot}93$

FIG. 13 and 14. The effect of mixing-length ratio on the velocity profile at the shroud outlet.

$$Re = 1{\cdot}2 \times 10^6, \frac{l}{d_1} = 0{\cdot}5, \frac{{}_tp_1}{p_\infty} = 2{\cdot}00, \frac{{}_tT_2}{{}_tT_1} = 1{\cdot}0$$

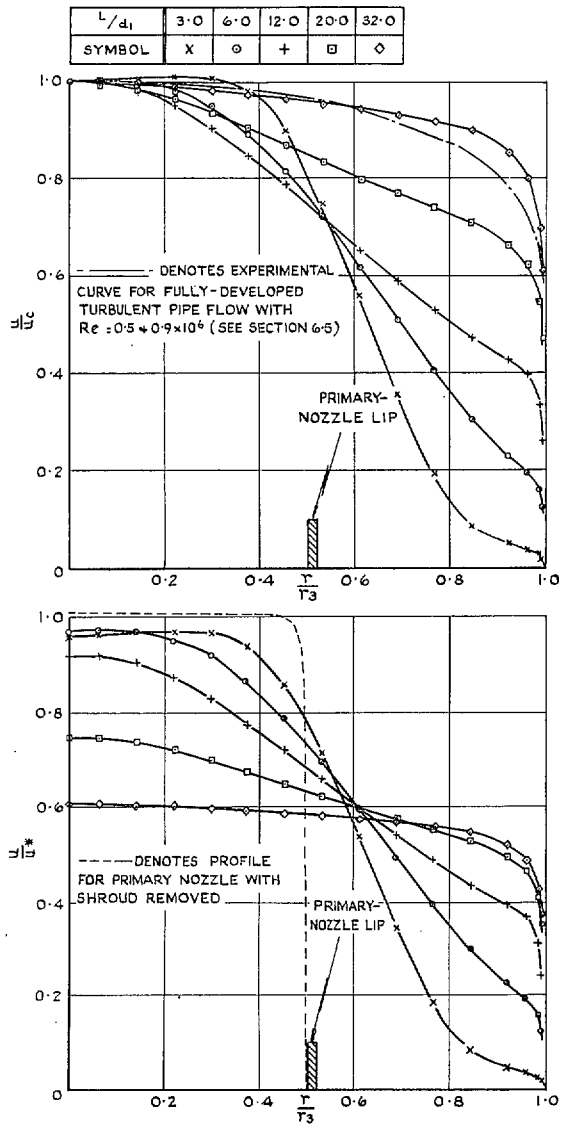

FIG. 15. The effect of mixing-length ratio on the velocity profile at the shroud outlet.

$$Re = 1{\cdot}2 \times 10^6, \quad \frac{l}{d_1} = 0{\cdot}5, \quad \frac{a_2}{a_1} = 2{\cdot}90,$$

$$\frac{{}_tp_1}{p_\infty} = 2{\cdot}00, \quad \frac{{}_tT_2}{{}_tT_1} = 1{\cdot}0$$

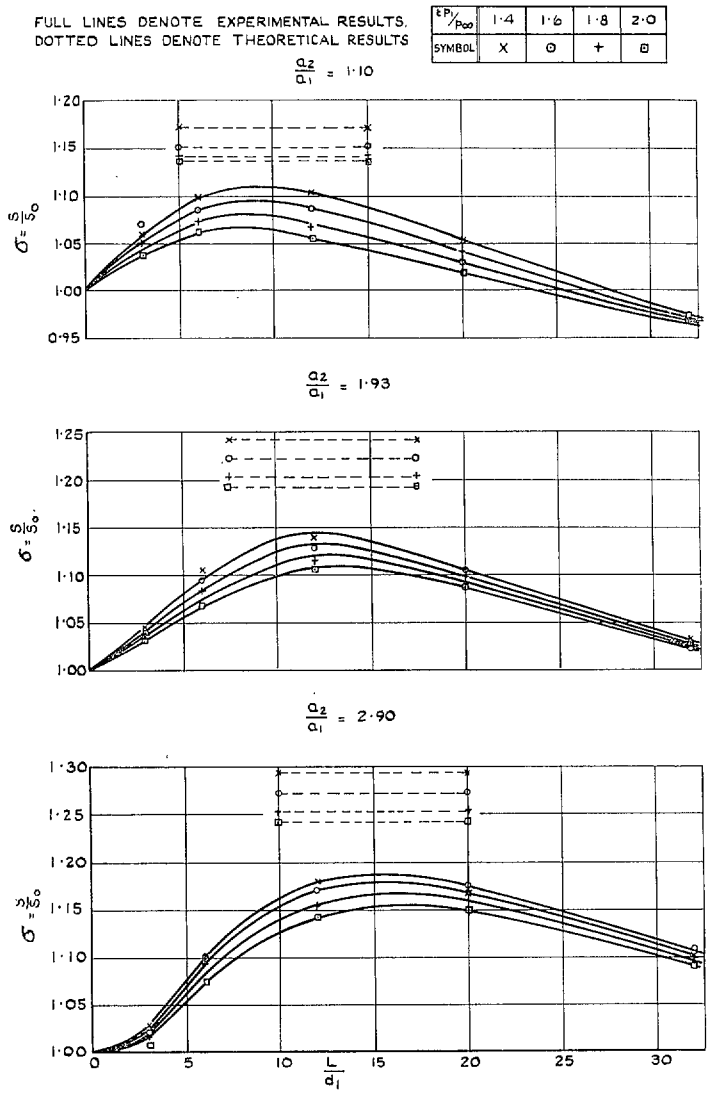

FIG. 16. The effect of mixing-length ratio, jet pressure ratio and ejector area ratio on the thrust parameter.

$$\frac{{}_tT_2}{{}_tT_1} = 1{\cdot}0, \quad \frac{l}{d_1} = 0{\cdot}5$$

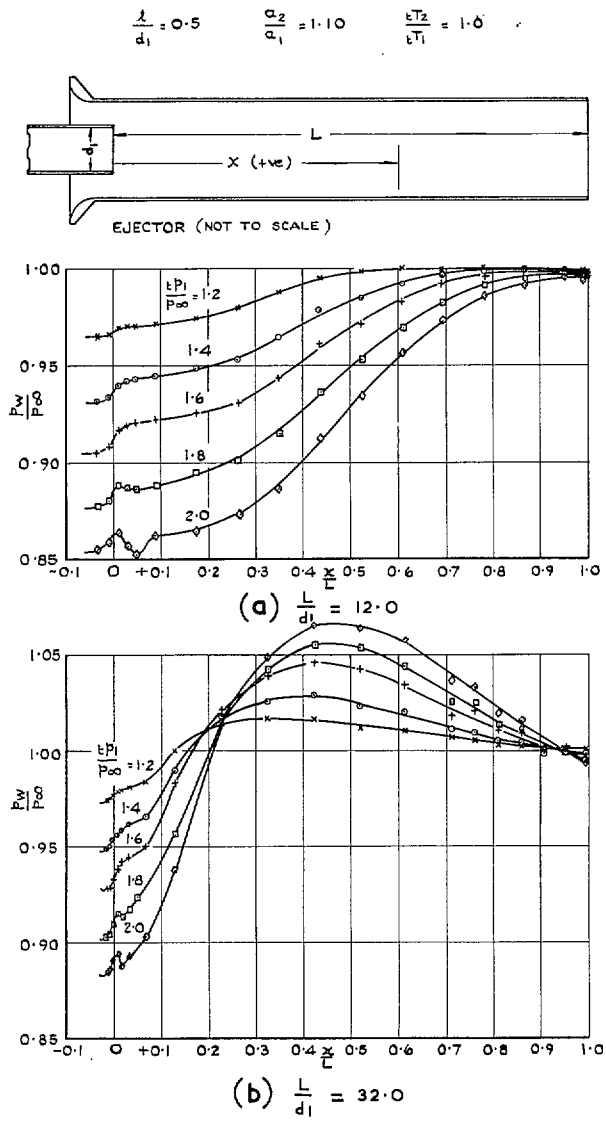

FIG. 17a and b. The effect of jet pressure ratio on the static-pressure distribution along the shroud wall.

$$\frac{l}{d_1} = 0{\cdot}5, \quad \frac{a_2}{a_1} = 1{\cdot}10, \quad \frac{{}_tT_2}{{}_tT_1} = 1{\cdot}0$$

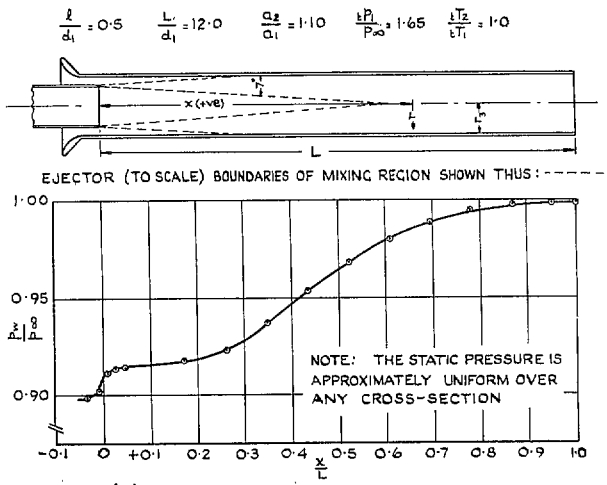

(a) THE STATIC-PRESSURE DISTRIBUTION.

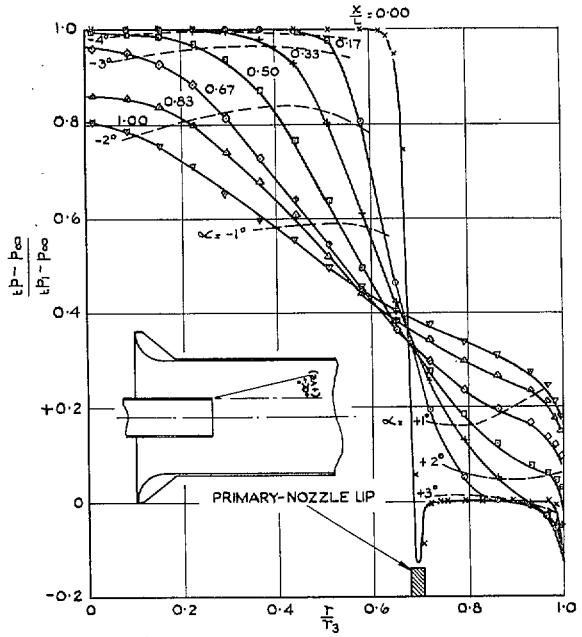

(b) THE TOTAL-PRESSURE DISTRIBUTION.

FIG. 18a and b. The development of the mixing process within the shroud.

$$\frac{l}{d_1} = 0{\cdot}5,\ \frac{L}{d_1} = 12{\cdot}0,\ \frac{a_2}{a_1} = 1{\cdot}10,$$

$$\frac{{}_tp_1}{p_\infty} = 1{\cdot}65,\ \frac{{}_tT_2}{{}_tT_1} = 1{\cdot}0$$

(86977) Wt.64/1857 K.5 6/63 Hw.

Publications of the Aeronautical Research Council

ANNUAL TECHNICAL REPORTS OF THE AERONAUTICAL RESEARCH COUNCIL (BOUND VOLUMES)

1942 Vol. I. Aero and Hydrodynamics, Aerofoils, Airscrews, Engines. 75*s.* (post 2*s.* 9*d.*)
Vol. II. Noise, Parachutes, Stability and Control, Structures, Vibration, Wind Tunnels. 47*s.* 6*d.* (post 2*s.* 3*d.*)

1943 Vol. I. Aerodynamics, Aerofoils, Airscrews. 80*s.* (post 2*s.* 6*d.*)
Vol. II. Engines, Flutter, Materials, Parachutes, Performance, Stability and Control, Structures. 90*s.* (post 2*s.* 9*d.*)

1944 Vol. I. Aero and Hydrodynamics, Aerofoils, Aircraft, Airscrews, Controls. 84*s.* (post 3*s.*)
Vol. II. Flutter and Vibration, Materials, Miscellaneous, Navigation, Parachutes, Performance, Plates and Panels, Stability, Structures, Test Equipment, Wind Tunnels. 84*s.* (post 3*s.*)

1945 Vol. I. Aero and Hydrodynamics, Aerofoils. 130*s.* (post 3*s.* 6*d.*)
Vol. II. Aircraft, Airscrews, Controls. 130*s.* (post 3*s.* 6*d.*)
Vol. III. Flutter and Vibration, Instruments, Miscellaneous, Parachutes, Plates and Panels, Propulsion. 130*s.* (post 3*s.* 3*d.*)
Vol. IV. Stability, Structures, Wind Tunnels, Wind Tunnel Technique. 130*s.* (post 3*s.* 3*d.*)

1946 Vol. I. Accidents, Aerodynamics, Aerofoils and Hydrofoils. 168*s.* (post 3*s.* 9*d.*)
Vol. II. Airscrews, Cabin Cooling, Chemical Hazards, Controls, Flames, Flutter, Helicopters, Instruments and Instrumentation, Interference, Jets, Miscellaneous, Parachutes. 168*s.* (post 3*s.* 3*d.*)
Vol. III. Performance, Propulsion, Seaplanes, Stability, Structures, Wind Tunnels. 168*s.* (post 3*s.* 6*d.*)

1947 Vol. I. Aerodynamics, Aerofoils, Aircraft. 168*s.* (post 3*s.* 9*d.*)
Vol. II. Airscrews and Rotors, Controls, Flutter, Materials, Miscellaneous, Parachutes, Propulsion, Seaplanes, Stability, Structures, Take-off and Landing. 168*s.* (post 3*s.* 9*d.*)

1948 Vol. I. Aerodynamics, Aerofoils, Aircraft, Airscrews, Controls, Flutter and Vibration, Helicopters, Instruments, Propulsion, Seaplane, Stability, Structures, Wind Tunnels. 130*s.* (post 3*s.* 3*d.*)
Vol. II. Aerodynamics, Aerofoils, Aircraft, Airscrews, Controls, Flutter and Vibration, Helicopters, Instruments, Propulsion, Seaplane, Stability, Structures, Wind Tunnels. 110*s.* (post 3*s.* 3*d.*)

Special Volumes

Vol. I. Aero and Hydrodynamics, Aerofoils, Controls, Flutter, Kites, Parachutes, Performance, Propulsion, Stability. 126*s.* (post 3*s.*)
Vol. II. Aero and Hydrodynamics, Aerofoils, Airscrews, Controls, Flutter, Materials, Miscellaneous, Parachutes, Propulsion, Stability, Structures. 147*s.* (post 3*s.*)
Vol. III. Aero and Hydrodynamics, Aerofoils, Airscrews, Controls, Flutter, Kites, Miscellaneous, Parachutes, Propulsion, Seaplanes, Stability, Structures, Test Equipment. 189*s.* (post 3*s.* 9*d.*)

Reviews of the Aeronautical Research Council

1939–48 3*s.* (post 6*d.*) 1949–54 5*s.* (post 5*d.*)

Index to all Reports and Memoranda published in the Annual Technical Reports

1909–1947 R. & M. 2600 (out of print)

Indexes to the Reports and Memoranda of the Aeronautical Research Council

Between Nos. 2351–2449	R. & M. No. 2450 2*s.* (post 3*d.*)
Between Nos. 2451–2549	R. & M. No. 2550 2*s.* 6*d.* (post 3*d.*)
Between Nos. 2551–2649	R. & M. No. 2650 2*s.* 6*d.* (post 3*d.*)
Between Nos. 2651–2749	R. & M. No. 2750 2*s.* 6*d.* (post 3*d.*)
Between Nos. 2751–2849	R. & M. No. 2850 2*s.* 6*d.* (post 3*d.*)
Between Nos. 2851–2949	R. & M. No. 2950 3*s.* (post 3*d.*)
Between Nos. 2951–3049	R. & M. No. 3050 3*s.* 6*d.* (post 3*d.*)
Between Nos. 3051–3149	R. & M. No. 3150 3*s.* 6*d.* (post 3*d.*)

HER MAJESTY'S STATIONERY OFFICE

from the addresses overleaf

Printed and published by
HER MAJESTY'S STATIONERY OFFICE

To be purchased from
York House, Kingsway, London W.C.2
423 Oxford Street, London W.1
13A Castle Street, Edinburgh 2
109 St. Mary Street, Cardiff
39 King Street, Manchester 2
50 Fairfax Street, Bristol 1
35 Smallbrook, Ringway, Birmingham 5
80 Chichester Street, Belfast 1
or through any bookseller

Printed in England

S.O. Code No. 23-3320